Geological Survey of Japan Cruise Report No. 21, p. 98–159, 1986

VIII. LOCAL VARIABILITY OF MANGANESE NODULE DEPOSITS AROUND THE SMALL HILLS IN THE GH81-4 AREA

Akira Usui

Introduction

Local variation of nodule occurrence, abundance, and morphology were investigated in a small model site located in the middle of the Central Pacific Basin. Detailed surveys have not been made around this area, because the Central Pacific Basin are not considered as a possible prime mining area. We have found a few high grade-nodule provinces locally distributed on the Wake-Tahiti Transect (USUI, 1982). As shown in Fig. VIII-1, the GH81-4 area is the second small model site on the transect following the GH80-5 area (NAKAO and MORITANI, 1984). The objective of this study is to characterize the pattern of local variation of manganese nodule facies and to find its relationships to the geology, which will be available in considering nodule formation process and in mineral exploration.

Bathymetrical and geological mapping was made along latitudinal and longitudal survey lines with intervals of 2.5 n.m. (ca. 4.5 km). During the first leg, nodule sampling was carried out using free-fall grabs at 33 stations at intersections of 5-nautical mile (ca. 9 km) grid as a regional survey of the GH81-4 area. During the second leg, nodule and sediment samplings were carried out using free-fall grabs, piston corers, box corers, and dredges in the two detailed survey areas. The shortest sampling interval in these survey areas is several hundred meters. Methods of sampling, sea-bed photography, and on-board nodule description employed are similar to those of the GH80-5 (USUI and NAKAO, 1984).

Survey area

The GH81-4 area (2°45′N-3°20′N, 169°25′W-169°50′W) is situated at low latitude zone of the Central Pacific Basin (Fig. VIII-2). This area includes st. 1635 of the GH80-1 cruise, where a local variation of nodule facies was expected. Topography is generally flat and abyssal hills are dominant. Water depth ranges from 5,000 to 5,500 meters. This area includes three abyssal hills of a few hundred meters elevation from the basin. The northern hill and southern hill were selected as detailed survey areas I and II respectively, based on results of the grid survey. The hill in the area I is apparently NNW-SSE trended and of asymmetric topography. The southwestern flank of it is much steeper (dip: 5-10°) than the opposite flank. Some steep sub-peaks at the southwestern end may be an elevated basaltic basement, because fresh basaltic rock fragments were collected from a few stations. The southern hill of the area II is also of asymmetric topography, having a steep western flank (dip: ca. 10°) and a N-S trended depression at the hill foot and an eastern gentle slope.

Most of these area are covered with surface siliceous ooze or clay, though older consolidated and unconsolidated sediments are sometimes exposed around hill tops

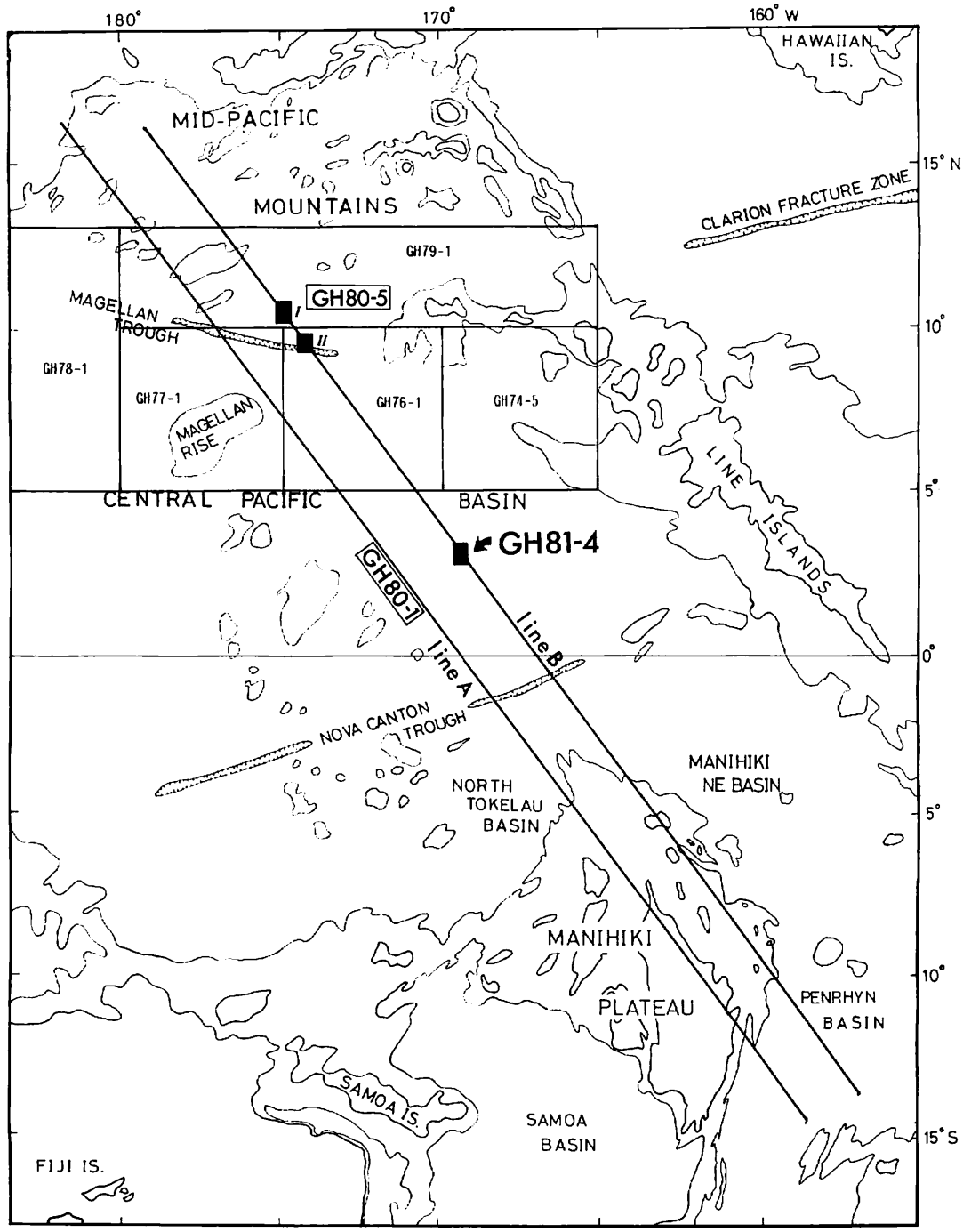

Fig. VIII-1 Location map of survey areas of the GH81-4 cruise and previous GSJ cruises. Contours denote 2000 and 2600 fathosms. Base map modefied from CHASE *et al.* (1977) published by SIO.

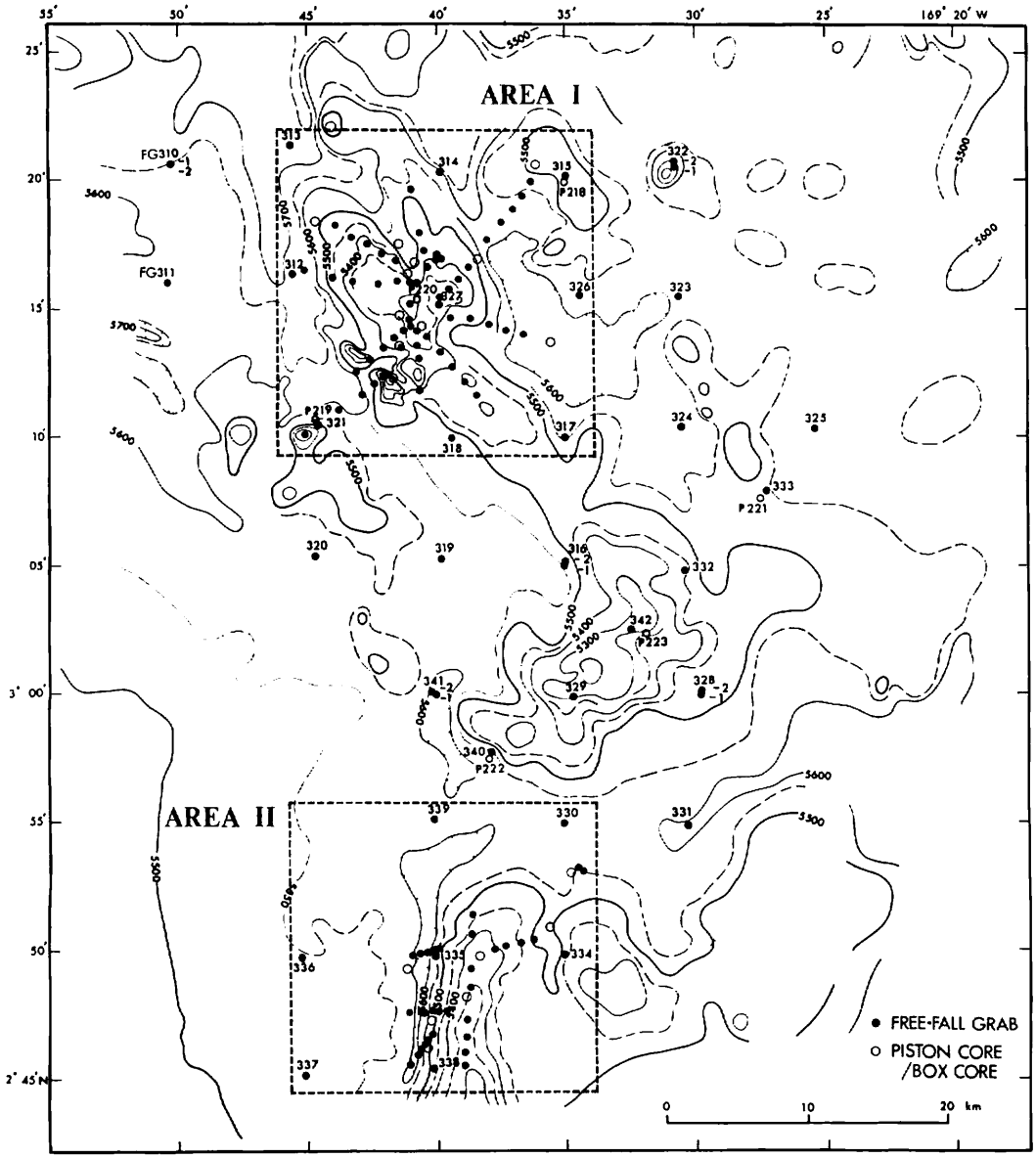

Fig. VIII-2 Topography and sampling stations of the GH81-4 area.

(NISHIMURA, this cruise report). Seismic profile records reveal that the uppermost acoustic transparent layer defined as Unit I is possibly correlated to the siliceous ooze and clay sequences from the Oligocene to the Recent (TANAHASHI, this cruise report). On the steep flanks, Units IIa, IIb, or acoustic basement are locally exposed, some of which may be identified as basal outcrop.

Nodule occurrence and morphology

Among 149 points of successful sampling, manganese nodules were obtained at 97 points (82 by free-fall grabs, 10 by box corers, 4 by piston core, and one by dredge). Occurrence of nodules on sediment surfaces can be viewed by one-shot cameras installed inside a free-fall grab or a box corer, and observed with surface sediments of recovered box cores. Nodule abundances, coverage ratios, external morphology, sea-bed occurrence, and other on-board data for all stations are listed in Appendix VIII-1 and -2.

The criteria for on-board nodule description established during previous GSJ cruises in the northern Central Pacific Basin (MORITANI *et al.*, 1977) was adopted and it proved available to the nodules of the GH81-4 area. All of collected nodules were classified according to surface structure into type s (smooth surface nodules), type r (rough surface nodules), and type s·r (nodules of intermediate surface feature). Intermediate feature is attributable to variable internal structure as revealed by microscopical study of split nodules (USUI, this cruise report); e.g., thinly developed gritty structure surrounding a smooth nodule or thinly developed smooth structure surrounding a gritty nodule. Very few nodules have different surface structure between nodule tops and bottoms.

Sea-bed photographs and on-site observation of box core surface show markedly different occurrences with nodule type. Typical rough surface nodules are commonly buried within the top siliceous sediments of several centimeters thickness. For in-

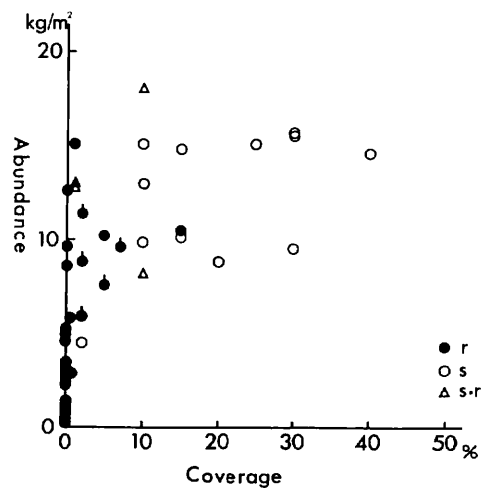

Fig. VIII-3 Relationships between nodule abundance and nodule coverage ratio revealed by sea-bed photography, showing differences with nodule type.

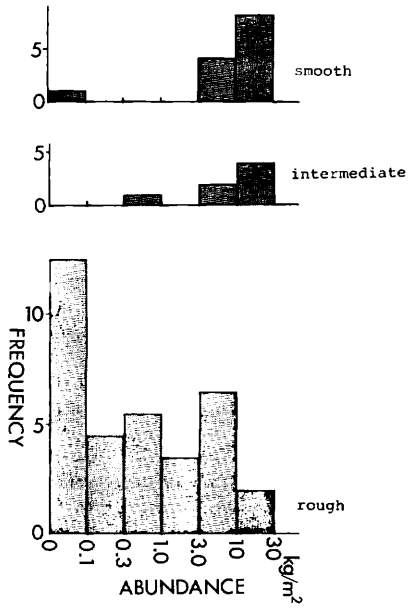

Fig. VIII-4 Frequency distribution of nodule abundance. Frequency is shown in numbers of stations of nodule occurrence.

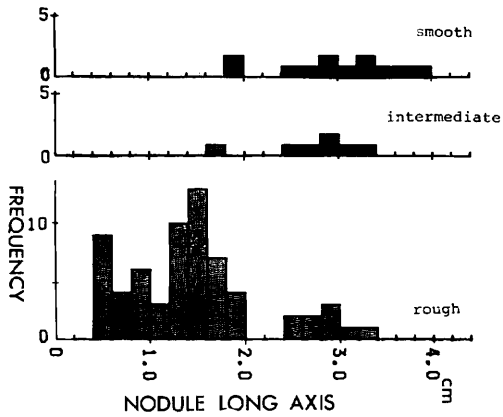

Fig. VIII-5 Frequency distribution of nodule diameter. Nodule long axis is represented by the median values of longest diameters in each station. Frequency is shown in numbers of stations of nodule occurrence.

Table VIII-1 Previous summary of manganese nodule characteristics in the Central Pacific Basin.

Nodule type	r	s
Abundance	<10 kg/m^2	10-20 kg/m^2
Mode of long axis	1-2 cm	2-4 cm
Occurrence on/in sediment surface	buried	exposed
Dominant shape	S, D	ID, IS, IDP
Internal structure	laminated, concentric, and symmetrical	massive, compact and surrounding layers
Internal cracks	rare	dominant
Polynucleation	rare	common
Dominant surface sediments associated	siliceous ooze or clay	pelagic or zeolitic clay

modified from Usui (1982)

stance, at FG327 many nodules (abundance: 4.5 kg/m^2) were samples despite no visible nodule on the sea-bed photograph (coverage: 0%). Fig. VIII-3 showing the relationship between nodule abundance and coverage well demonstrates a burial tendency of the r-type nodules. Frequency distribution of abundance (Fig. VIII-4) and median size (Fig. VIII-5) show a remarkable difference with nodule type. The size of r-type nodules is relatively small ranging from 1 mm to 2 cm, and the abundance quite

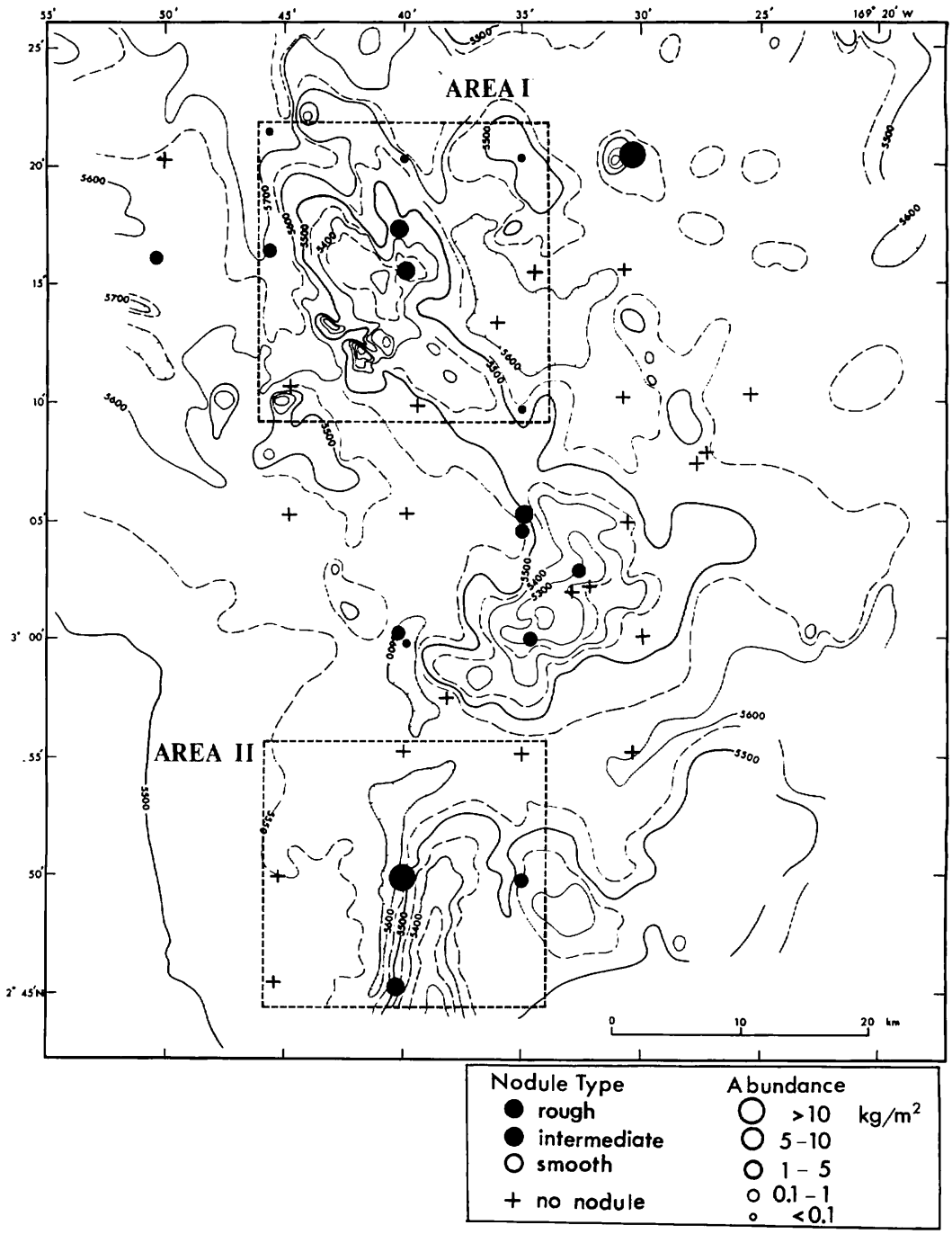

Fig. VIII-6 Distribution of manganese nodules in the GH81-4 area. Data from detailed survey areas I and II are not included.

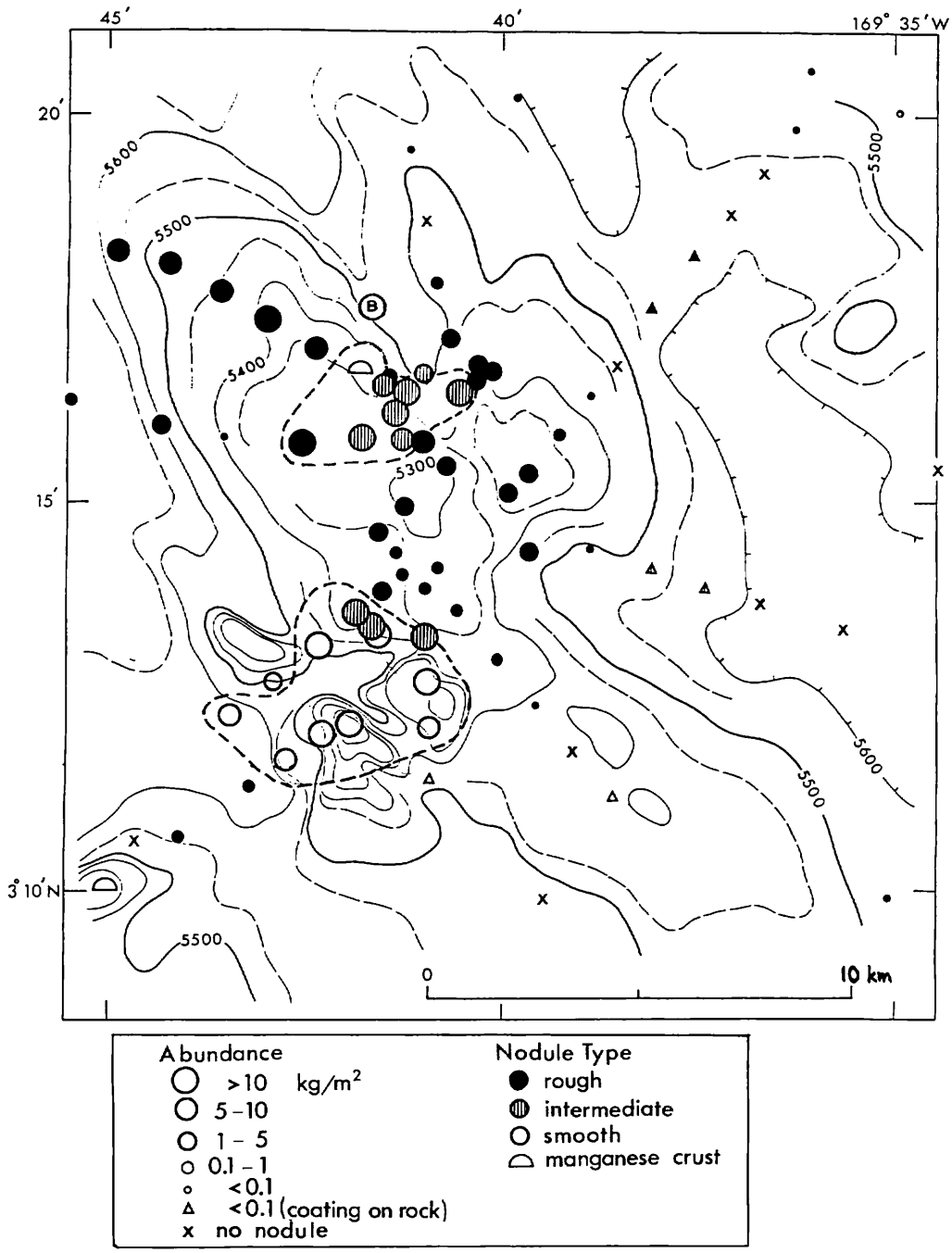

Fig. VIII-7 Distribution of manganese nodules in Area I. Dashed lines on the map indicate areas of greater nodule coverage than 5% on sea-bed photographs. Symbol B in a circle: nodules buried at 15 cm depth of box core B63.

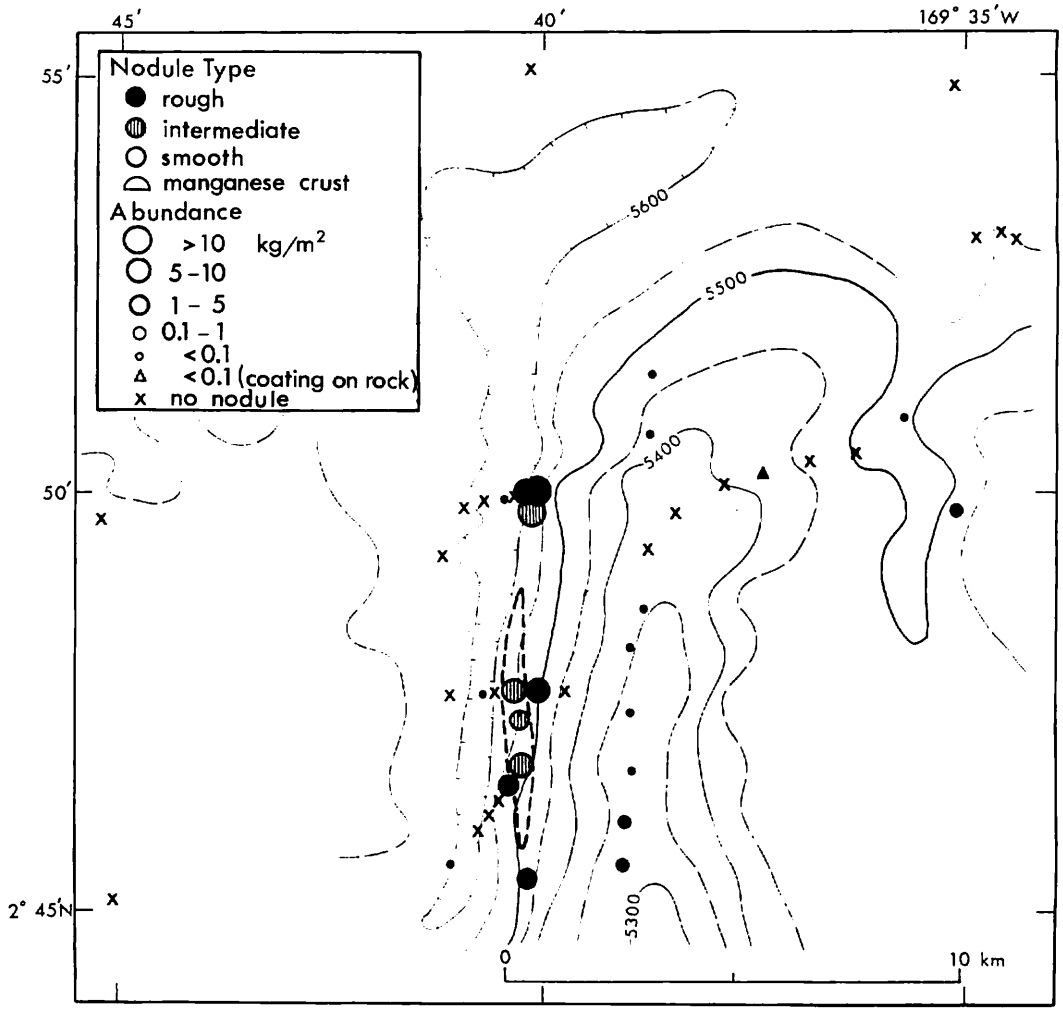

Fig. VIII-8 Distribution of manganese nodules in Area II. Dashed lines on the map indicate areas of greater nodule coverage than 5% on sea-bed photographs.

variable. Their shape is mostly spherical or discoidal, and mononucleated nodules are dominant. On the other hand, typical s-type nodules are usually exposed to sea water, and almost all nodules on the sea floor are visible on the sea-bed photographs. The size of s-type nodules is relatively large ranging from 2 cm to 4 cm, and the abundance is usually greater than that of r-type nodules. The shape is variable, and polynucleated feature is dominant. Nodules of intermediate surface structure generally have intermediate characteristics between s-type and r-type nodules, in terms of sea floor occurrence, size, and abundance.

These tendency of sea-bed occurrence and physical characteristics of manganese nodules of the GH81-4 area are generally similar to those found in the northern Cen-

tral Pacific Basin during the GH76-1, GH77-1, and GH80-1 cruises (MORITANI *et al.*, 1977; USUI, 1979; USUI, 1982). Table VIII-1 shows a summary on characteristics of the two nodule types in comparison with the GH81-4 nodules.

Local variation of manganese nodule facies

Variation of manganese nodules in abundance, coverage, morphology, chemistry, and mineralogy have been reported on various scales; from hundred meters to thousand kilometers (ANDREWS and FRIEDRICH, 1979; HALBACH and ÖZKARA, 1979). It was found on the Wake-Tahiti Transect (4,000 km long) in the Central Pacific that nodule morphology varies from type s to type r in accordance with four geologic provinces, and this regional variation is due to the variation of nodule mineralogy resulting in different morphological features (smooth and rough surfaces) and compositional variation (USUI and MOCHIZUKI, 1982). In the GH81-4 area a great variation of nodule facies was found on the scale of kilometers. It is interesting that this short-scale variation in occurrence and morphology is equivalent to above-mentioned regional variation.

Manganese nodules are abundant in top, flank and foot of abyssal hills, and are barren or scarce in the flat basin area off the hills (Fig. VIII-6). Nodule occurrence and morphology are not uniform but quite variable around these hills (Figs. VIII-7 and 8). Detailed surveys reveal that the scale of variation of nodule type is less than the interval of survey grid (ca. 9 km). All the types s, s·r, and r occur locally in these areas. Especially type s and s·r are characteristically distributed in small and isolated areas of several kilometers across in the Areas I and II.

Detailed survey: Area I

Nodules of greater abundance than 1 kg/m^2 are distributed near the top and on the western flank of the hill, and nodules are rare in the basin areas deeper than approximately 5,500 m. The r-type nodules dominate in this area, their abundance ranging from trace to 11 kg/m^2. The s-nodules and intermediate-surface nodules are abundantly (greater than 10 kg/m^2) distributed in two isolated areas each extending only several kilometers across. Two enclosing dashed lines in Fig. VIII-7 denote areas of greater nodule coverage than 5 %. As stated in the previous section, s-type nodules occur exposed to sea water. High nodule coverage areas and areas of s-type nodules are consequently overlapped. Nodules of type s·r from the northern part of the hill comprise very thin gritty coating on older smooth nodules, whereas nodules of type s from the southwestern sub-peaks are of typical smooth surface.

These nodules are always associated with unconsolidated siliceous ooze, except for manganese crusts from FG359 and FG354. At the point FG359 nearly at the top of a small peak no nodule was collected, but sea-bed photography suggests presence of a hard rocks coated with manganese oxides. At the point FG354 no nodule was also collected, but the sea-bed photograph shows some sediments and a large block of hard rock fragments which is probably similar to large rock fragments collected by the dredge D496.

Detailed survey: Area II

Manganese nodules are distributed on the top and on the western steep slope. The r-type nodules dominate in this area though the abundance considerably varies (Fig. VIII-8). Nodules are barren in the flat basins off the hill as well as in the Area I. Abundance of r-type nodules is very low on the hill top (maximum: 0.4 kg/m^2 in FG394) and in the western depression at the hill foot (e.g., 0.4 kg/m^2 in FG401). The greatest abundance is encountered on the western flank, but many of the r-type nodules contain older s-type nodules inside. Intermediate-surface nodules which are composed of inside s-type nodules and thin gritty coatings show a strikingly narrow distribution on the flank. The area of greater nodule coverage than 5 percent overlaps the area of abundant occurrence of intermediate type.

These patterns of local variation of nodule facies are generally common in areas I and II. Factors determining these characteristic distribution patterns would be considered in relation to the present and past sedimentary history on the basis of seismic survey and sediment stratigraphy. Results of this survey suggest that water depth is no major factor controlling nodule variation as PAUTOT and MELGUEN (1979) proposed in the Southwest Pacific. Surface sediment distribution reveals no significant association with nodule facies, though the age of top sediment is variable around the hill (NISHIMURA, this cruise report).

Apparently most relating geological factor is the stratigraphy of substrates. On the hill tops in Areas I and II the Tertiary siliceous sediments partly outcrop, suggesting no sedimentation and/or deep-sea erosion in the Quaternary time (NISHIMURA, this cruise report). Seismic profile records reveal that young sediments characterized by acoustic transparent layers is much thinner around the hills (TANAHASHI, this cruise report) in accordance with sedimentological results. It is also a remarkable evidence of local variation patterns that smooth surface nodules are apt to develop abundantly where the uppermost transparent layer is lacking or scarce (USUI and TANAHASHI, this cruise report). These characteristics of substrates suggest a close relationship of nodule growth to sedimentary history. It is in general applicable in the GH81-4 area that a very rapid sedimentation of biogenic detritus prevents nodule growth, whereas slow sedimentation is favorable for it. Following possibilities could be pointed out on the growth of s-type nodules; that nodule growth is preferentially promoted at a time of erosion by strong bottom current, and that nodules are continuously growing at a continuous slow sedimentation during upward lifting of nodules. However, the age and rate for nodules of each type and those of associated sediments should be comparatively investigated, before we conclude the relationship of nodule growth to sedimentary history.

Buried nodules

Besides the nodules on sediment surface mentioned above, some nodules were collected deep within a box core and piston cores as (Appendix VIII-3). They are considered from their occurrence to be lain in-situ within the sediments. Four cores (B63, P218, P224, P225) contain manganese nodules, most of them are of type s except for those from P218. The manganese oxide aggregates found within the piston core P218 at a depth of 30 to 35 cm from sediment top are odd-shaped; rod, pipe, plate, and den-

drites (Appendix VIII-3). Their chemistry (USUI and TERASHIMA, this cruise report) and mineralogy (USUI, this cruise report) suggest that they are not normal deep-sea manganese nodules such as types s or r, but formed under anomalous conditions. The composition is similar to those from submarine hydrothermal deposits (LONSDALE *et al.*, 1980) and shallow-water diagenetic deposits. Although we have not further detailed geochemical or geological data now, this material was noticed because it suggests hydrothermal activity during the deposition of Unit I.

Summary

Detailed survey with free-fall grabs, piston corers, box cores, and sea-bed photography during the GH81-4 cruise have shown a pattern of local variation of nodule facies around abyssal hills of the equatorial Central Pacific Basin. Nodules are abundant on and around the hills but rare in the basin areas off the hills. Nodule types previously described regionally in the Central Pacific are also distributed in this small area, though areal distribution of each type is variable. Especially smooth surface nodules (including type s and s·r) occupy only areas of several kilometers across. In spite of complicated areal nodule distribution pattern, mutual relations among the sea-bed occurrence, morphology, abundance, and size of each type are similar to those from northern Central Pacific Basin and Wake-Tahiti Transect.

Therefore the factors controlling nodule type variability may be common on local and regional scales. Water depth or surface sediment type do not seem a major controlling factor, but sedimentary history to be established on the basis of acoustic and sediment stratigraphy may be the most relating factor. Further comparative study of nodule age and rate with those of associated sediments is needed in order to correlate any sedimentological condition to nodule growth process.

References

ANDREWS, J. E. and FRIEDRICH, H. W. (1979) Distribution patterns of manganese nodule deposits in the Northeast Equatorial Pacific. *Marine Mining*, vol. 2, no. 1/2, p. 1-43.

HALBACH, P. and ÖZKARA, M. (1979) Morphological and geochemical classification of deep-sea ferromanganese nodules and its genetical interpretation. *In* C. LALOU (ed.) *La Genèse des Nodules de Manganèse*. C. N. R. S. Rept. no. 289, p. 77-88.

LONSDALE, P., BURNS, V. M. and FISK, M. (1980) Nodules of hydrothermal birnessite in the caldera of a young seamount. *J. Geol.*, vol. 88, p. 611-618.

NAKAO, S. and MORITANI, T. (eds.) (1984) Marine Geology, Geophysics and Manganese Nodules in the Northern Vicinity of the Magellan Trough, August-October 1980 (GH80-5 Cruise). *Geol. Surv. Japan Cruise Rept.*, no. 20, p. 1-272.

MORITANI, T., MARUYAMA, S., NOHARA, M., MATSUMOTO, K., OGITSU, T. and MORIWAKI, H. (1977) Description, classification, and distribution of manganese nodules. *Geol. Surv. Japan Cruise Report*, no. 8, p. 136-158.

PAUTOT, G. and MELGUEN, M. (1979) Influence of deep water circulation and sea floor

morphology on the abundance and grade of Central South Pacific manganese nodules. *In* BISCHOFF, J. L. and PIPER, D. Z. (*eds.*), *Marine Geology and Oceanography of the Pacific Manganese Nodule Province*, Plenum, New York, p. 437–473.

USUI, A. (1979) Minerals, metal contents and mechanism of formation of manganese nodules from the Central Pacific Basin (GH76–1 and GH77–1 areas). In: BISCHOFF, J. L. and PIPER, D. Z. (Eds.), *Marine Geology and Oceanography of the Pacific Manganese Nodule Province*, Plenum, New York, pp. 651–677.

——— (1982) Variability of manganese nodule deposits: the Wake-Tahiti Transect. *Geol. Surv. Japan Cruise Rept.*, no. 18, pp. 138–223.

——— and MOCHIZUKI, T. (1982) Regional variation of manganese nodule chemistry from Wake to Tahiti, GH80–1 cruise. *Geol. Surv. Japan Cruise Report*, no. 18, p. 338–354.

——— and NAKAO, S. (1984) Local variability of manganese nodule deposits in the GH80-5 area. *Geol. Surv. Japan Cruise Rept.*, no. 20, p. 106–164.

Appendix VIII-1 Sample list and results of on-site observations of manganese nodules.
tr: less than 0.05 kg/m^2
—: no available data.
( ): doubtful data.
Sediment type, s: siliceous, c: calcareous, O: ooze, C: clay.
Sediment consistency, H': hit nodules, H: hard, M: medium, L: loose.

Station/Sample No.	Sediment type	Sea-bed photograph Nodule coverage (%)	Sea-bed photograph Sediment consistency	Morphological type	Abundance (kg/m^2)	Size distribution (nos.) 10	8-10	6-8	4-6	2-4	1-2	1cm
2576 FG310-1	SO	0	-		0							
-2	SO	0	-		0							
2577 FG313	SC	0	L	Sr	0.1						3	2
2578 FG314	SC	0	L	Sr	0.1						1	5
2579 P218	SO	-	-	Vs, Vs+r	-							
FG315	SC	0	L	Sr	0.1						2	2
2580 FG322-1	SC	1	-	IDs·r, ISs·r, Ds·r	12.8			5	6	21	16	26
-2	-	15c	L	IDs·r	0.4					3		
2581 FG311	SO	0	L	Dr	0.2					1	0	1
2582 FG312	SO	0	-	Sr	0.8					5	8	3
2583 P220	SO	-	-	Sr	-							1
FG327	SO	0	-	Sr	4.5				2	12	26	
2584 FG326	SO	0	-		0							
2585 FG323	SO	0	M		0							
2586 P219	SC	-	-		0							
FG321	-	-	-		-							
2587 FG318	SC	0	L		0							
2588 FG317	SC	0	L	Sr	0.1					1	0	1
2589 FG324	SO	0	L		0							
2590 FG325	SO	0	-		0							
2591 P221	SC	-	-		0							
FG333	SO	0	L		0							
2592 FG320	SO	0	L		0							
2593 FG319	-	0	L		0							
2594 FG316-1	SO	0	L	Sr, Dr	0.1					1	4	1
-2	SC	0	L	IDr, IDPr	2.1			1	2	22	2	1
2595 FG332	SC	0	-		0							
2596 P223	SC	-	-		0							
FG342	SO	0	-	Sr	0.4					1	13	15
2597 FG341-1	SO	0	L	Sr	0.3					1	12	8
-2	-	0	L	Sr	0.1						2	
2598 FG329	-	0	L	Sr	0.8					5	9	
2599 FG328-1	SO	0	L		0							
-2	SO	0	L		0							
2600 P222	SC	-	-		0							
FG340	SO	0	-		0							
2601 FG339	SC	0	L		0							
2602 FG330	SO	0	-		0							
2603 FG331	SO	0	L		0							
2604 FG336	SO	0	-		0							
2605 FG335	-	0	-	DPs·r, Ts·r, Fs·r, Ds·r, Fr	12.6	1	1	1	2	3	3	3
2606 FG334	SC	0	-	Sr	0.3					1	11	4
2607 FG337	SC	0	L		0							
2608 FG338	SC	0	-	Sr	4.9				5	3	48	20
2609 FG343	SO	0	L	Sr	1.3					5	34	17
2610 FG344	SO	0	-	Sr	0.1						5	
2611 FG345	SO	0	L	Sr	0.1						1	
2612 FG346	SO	0	-		0							
2613 B57	SO	(0)	-	Vr	0.1					1		
2614 FG347	SO	0	L	Vr	0.1							1
2615 FG348	SO	0	L		0							
2616 FG349	SO	0	-		0							
2617 FG350	SO	0	L	frag. of Dr	0.1						1	
2618 B58	SO	(0)	-	Sr	0.1							2
2619 FG351	SC	<1	M	Sr, Dr	2.8			1	0	9	50	12

Total weight (g)	Buried depth (cm)	Internal structure	Nucleus	Polynucleation (%)	Associated material Remarks on occurrence
0				-	pumice
0				-	do.
7				0	do.
3				0	
0	32			-	
3				0	
1482		compact layers surrounding rocks or broken nodules	altered basalt	10	zeolite aggregate?
45		compact and laminated layers surrounding rocks		0	
21		1-2 mm thick gritty layers surrounding rocks	soft clayey rock	0	
93		concentric and laminated	none or small	0	shark teeth
1				(0)	
527		concentric and laminated		0	
0				-	
0				-	
0				-	
-				-	(unsuccessful)
0				-	
8				0	shark tooth
0				-	
0				-	
0				-	
0				-	
0				-	
0				-	
14		concentric and laminated	none or small	0	
226		gritty 2 mm thick layers surrounding broken nodules	brown rock	10	
0				-	
0				-	
43		concentric and laminated	none or small	0	shark tooth
35			do.	0	
4				0	
97		concentric and laminated	none or small	0	
0				-	
0				-	
0				-	
0				-	
0				-	
0				-	
0				-	
0				-	
1457		complicated(inner compact, outer laminated)	zeolite aggregate	10	
38		concentric and laminated	none or small	0	
0				-	
569		concentric and laminated	none or small	0	
152		concentric and laminated	none or small	0	shark teeth
16				0	
2				0	
0				-	
1		thin coating on pumice	pumice	0	
1		do.	do.	0	
0				-	
0				-	
1				0	
1				0	pumice
329		concentric and laminated		0	

Appendix VIII-1 (continued)

Station/Sample No.	Sediment type	Sea-bed photograph: Nodule coverage (%)	Sea-bed photograph: Sediment consistency	Morphological type	Abundance (kg/m^2)	Size distribution (nos.): 10	8-10	6-8	4-6	2-4	1-2	1cm
2669 B65	SO	0	-	Sr	0.4						20	>100
2670 FG424	SO	0	L	Sr	3.3			1	1	9	16	7
2671 FG425	SO	-	-	Dr	tr						2	3
2672 FG426	SO	0	L	Fr	tr							2
2673 FG427	SO	-	-	Vr	0						1	
2674 FG428	SO	0	L		0							
2675 P230	SC	-	-		0							
2676 P226	SO	-	-		0							
FG393-1	SO	0	-		0							
-2	SO	0	L		0							
2677 FG394	-	0	L	Sr	0.4					1	14	7
2678 FG395	SO	-	-	Sr	0.1						6	2
2679 FG396	SO	0	L	Sr	0.1						1	2
2680 FG397	SO	0	L	Sr	0.1						2	
2681 B66	SC	0	L	Sr	0.1						3	8
2682 FG398	SO	0	L		0							
2683 FG399	SO	0	L		0							
2684 FG400	SO	0	L	Sr	0.1							6
2685 FG401	-	-	-		(0)							
2686 FG402	SO	0	L	Dr, SEr, IDr, Fr	8.6			4	10	3	1	
2687 FG403	SO	1	L	IDr, Dr	15.1	1	2	4	8	0	1	
2688 P227	SC	-	-		0							
2689 FG404	SO	0	L		0							
2690 FG405	SO	0	L	Sr	tr					1	2	
2691 FG406	SO	0	-		0							
2692 FG407	SO	5	L	IDs·r, Fs·r	7.6				8	40	1	
2693 FG408	SO	-	-	Sr, SEr	5.7		1	2	0	2	11	
2694 FG409	SO	0	L		0							
2695 B67	SO	(2)	-	IDr, Fr	3.3				5	24		
2696 FG410	SO	0	-	Sr	0.1						1	2
2697 FG411	SO	-	-		0							
2698 FG412	SO	0	-	Dr	tr						1	
2699 FG413	SO	0	L	Dr	tr						2	2
2700 P228	SO	-	-		0							
2701 FG414	SO	0.	L		0							
2702 FG415	SO	0	-	Vr	(0)					1		
2703 FG416	SO	0	L		0							
2704 FG417	SO	0	M		0							
2705 B68	SO	0	-	Sr	tr							2
2706 FG418	SO	0	M	Sr	0.1						5	1
2707 FG419	SO	0	L		0							
2708 FG420	SO	0	L		0							
2709 FG421	SO	0	L		0							
2710 FG422	SO	0	L	Dr, IDr	0.2					4	1	1
2711 FG423	SO	7	-	IDs·r, IDPs·r	9.6			2	16	39	1	
2712 P229	SC	-	-	IDr, IDPr	-					2		
2713 D496	-	-	-	Sr, Dr, IDs Crust	-							

Total weight (g)	Buried depth (cm)	Internal structure	Nucleus	Polynucleation (%)	Associated material Remarks on occurrence
61		do.	do.	0	all nodules buried
387		do.	do.	0	
3				0	
1				0	
2		thin coating on rocks		-	
0				-	
0				-	
0				-	
0				-	
0				-	
46		concentric and laminated	none or small	0	
12		do.	do.	0	
10		do.	do.	0	
7		do.	do.	0	
11		do.	do.	0	all nodules buried
0				-	
0				-	
3				0	shark tooth
0				-	
994		concentric laminated layers on rocks or nodule fragments	small rock fragments	10	
1740		do.	zeolite aggregate, shark tooth	10	
0				-	
0				-	
3				(0)	
0				-	
884		laminated layers on nodule fragments	soft clayey rocks	10	
659		concentric and laminated, compact layer around nuclei	do.	0	
0				-	
500		laminated layers on nodule fragments or rocks	zeolite aggregate	10	some nodules exposed
8		concentric and laminated	none or small	(20)	
0				-	
2				(0)	
4				0	
0				-	
0				-	
10		thin coating on whale ear bone	whale ear bone	(0)	
0				-	
0				-	
1				(0)	
8		concentric and laminated	none or small	(20)	
0				-	
0				-	
0				-	
27		concentric laminated layers on nodule fragments	none	0	
1111		do.	none	20	
19		do.	none	(50)	
~160kg		variable	shark teeth, whale ear bone	(0)	zeolitic claystone

(Note) Sediment type/ S: siliceous, C: clay, O: ooze
Coverage/ figure with c: Mn crust
Consistency/ H: hit nodules, M: medium, L: low
"-"denotes no available data.

Appendix VIII-1 (continued)

Station/Sample No.	Sediment type	Sea-bed photograph: Nodule coverage (%)	Sea-bed photograph: Sediment consistency	Morphological type	Abundance (kg/m^2)	Size distribution (nos.): 10	8-10	6-8	4-6	2-4	1-2	1cm
2620 FG352	SC	0	L	Sr, Dr	9.6				6	33	57	13
2621 FG353	SC	30	-	ISPs, IDPs, IDs Is	15.6			3	32	55	1	
2622 B59	SC	30	M	IDPs, DPs	15.7			5	18	83		
2623 FG354	-	40c	M		0							
2624 FG355	SC	0	M	Sr, Dr	5.2				4	28	3	4
2625 FG356	SC	2	-	Sr, Dr	11.4				1	75	33	6
2626 FG357	SC	-	-	Sr	5.9				3	30	43	2
2627 FG358	SC	<1	M	Sr	5.8				2	27	31	5
2628 B60	SC	2	M	Sr	8.8				2	79	27	
2629 FG359	-	50c	H'		(0)							
2630 FG360	SC	0	-	Sr	0.3					2	6	4
2631 FG361	SO	1	L	Sr	0.2					1	7	
2632 FG362	SO	10	L	IDs, IDPs	9.9				9	74	8	
2633 FG363	SO	25	M	IDs, IDPs	15.1				17	104	38	4
2634 B61	SC	40	H'	IDs, IDPs, Fs	14.6				11	149	12	
2635 FG364	SO	15	-	IDs, IDPs, Is	10.2		1	3	5	40	29	
2636 FG365	SO	0	M	Sr	3.0				2	10	40	16
2637 FG366	SO	0	-	Sr	0.6					4	14	
2638 FG367	SO	0	-	Sr	1.3					11	31	
2639 B62	abandoned for winch trouble				-							
2640 FG368	SC	15	-	Ds, DPs, IDs	14.8	1	1	4	20	29		
2641 FG369	SO	0	L	Sr	1.7					9	27	12
2642 FG370	SO	0	L	Sr	0.2					3	5	1
2643 FG371	SO	0	L		0							
2644 FG372	SO	0	L	Sr	0.1						4	5
2645 B63	SC	(0)	-	IDs, IDPs	>12			1	19	131	6	
2646 FG373	SO	2	L	IDr, IDPr, Fr	4.9				8	25	7	6
2647 FG374	-	-	-	fragment of IDs?	tr							1
2648 FG375	SO	5	M	Sr, Dr	10.2				4	50	39	4
2649 FG376	SO	15	L	Sr, Dr	10.4			1	5	44	9	4
2650 FG377	SO	10	L	IDs·r, Ss·r, Ts·r	8.1			4	3	23	1	
2651 P224	SO	-	-	Ss	-					1		
2652 FG378	SO	30	L	IDs, IDPs	9.5				9	68	75	7
2653 FG379	SO	2	L	IDs	4.0			1	2	27	34	
2654 FG380	SO	10	M	IDs, IDPs	15.1				26	77	5	
2655 FG381	SO	10	-	Ss·r, Ds·r, Fs·r IDs·r	18.0				11	90	9	
2656 FG382	SO	0	L	Sr	0.5					2	7	6
2657 B64	SO	(0)	-	Sr	1.1			1	0	4	5	1
2658 FG383	SO	0	L	Vs	tr							3
2659 FG384	-	20	M	IDs, Ts	8.9			5	9	18	1	
2660 FG385	SO	10	-	IDs, ISs, Vs	13.0		3	3	7	25	7	
2661 FG386	SO	-	-	Ss·r, Ds·r	10.5				3	55	25	4
2662 FG387	SO	-	-	Sr	0.8					6	17	6
2663 P225	SO	-	-	Ds·r	-					1		
2664 FG388	SO	0	L	Vs	0.03						1	
2665 FG389	SO	0	L		0							
2666 FG390	SO	0	L	Dr	tr					1	1	
2667 FG391	SO	0	L	Sr	0.3					1	3	2
2668 FG392	SO	0	L	Sr	0.9					3	22	7

Total weight (g)	Buried depth (cm)	Internal structure	Nucleus	Polynucleation (%)	Associated material Remarks on occurrence
1110		do.		0	
1800		laminated layers on rocks or nodule fragments	zeolite aggregate	90	
2381			rock fragments	20	all nodules exposed
0				-	
605		concentric and laminated	none or small	5	
1314		concentric and laminated, outer layers rather massive	do.	5	
679		do.	do.	0	
671		concentric and laminated	do.	0	
1344		concentric and laminated outer layers rather massive	do.	5	shark teeth most nodules buried
0				-	
30		concentric and laminated	none or small	0	shark teeth
21		do.	do.	0	
1146		compact surrounding layer on rocks	altered basaltic rocks	50	
1742		compact layers surrounding rocks or nodule fragments	do.	50	
2214		do.	do.	20	all nodules exposed
1179		do.	zeolite aggregate	20	
347		concentric and laminated	none or small	0	
65		do.	do.	0	
149		do.	none, small, or shark tooth	0	
-				-	
1712		compact laminated on layers	zeolite aggregate?	40	
192		concentric and laminated	none or small	0	
29		do.	do.	0	
0				-	
8		concentric and laminated	none or small	0	
1811	15	compact layers surrounding nodule fragments	altered basalt?	50	8 nodules (84g) from bottom
565		do.	do.	20	
1				-	
1179		inner concentric layers and outer compact thin layers	none or small	0	
1206		slightly laminated compact layers	brown rocks	0	
938		inner concentric layers and outer compact thin layers	do.	30	
18		compact concentric layers	none or small	(0)	3 nodules (7g) from 694cm
1095		compact laminated layers surrounding rocks	altered basaltic rocks	70	
457		do.	do.	10	
1744		compact laminated layers surrounding rocks or nodule fragments	zeolite aggregate	50	
2084		compact laminated layer surrounding concentric layers	none or small	10	
53		concentric and laminated	do.	0	
163		do.	do.	0	
1		compact layers surrounding rocks	brown rocks	0	all nodules buried
1024		compact layers surrounding rocks or nodule fragments	none	0	
1500		do.	basaltic rocks?	5	
1216		do.	none or small	0	
90		concentric and laminated	do.	0	
61		thin compact layer surrounding concentric layers	do.	(0)	1 nodule (2g) from 720cm
4		do.		-	
0				-	
5				0	
33		concentric and laminated	none or small	0	
100		do.	do.	0	

GRID SURVEY

2576 FG310-1

0.0 kg/m² 0 % -

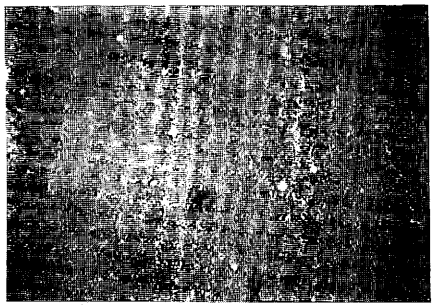

2576 FG310-2

0.0 kg/m² 0 % -

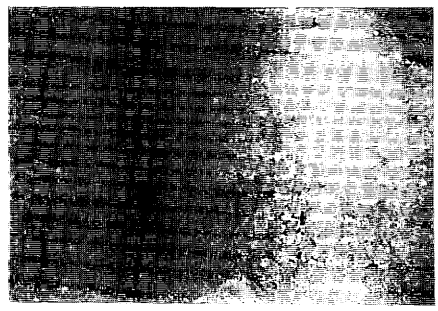

2577 FG313

0.1 kg/m² 0 % Sr

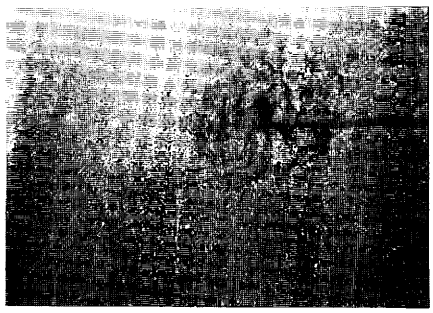

2578 FG314

0.1 kg/m² 0 % Sr

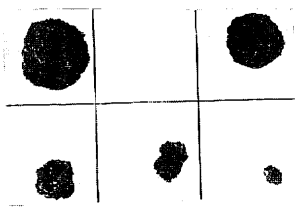

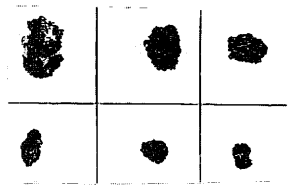

Appendix VIII-2(1)

Appendix VIII-2 Sea-bed occurrence and external morphology of manganese nodules. Each title includes station and sample numbers (first row) and abundance, seafloor coverage, and morphological type (second row). Data with ( ) doubtful. Diameter of trigger weight in sea-bed photos is ca. 10 cm. Scale mesh and bar with nodule samples: 25 mm.

2579 FG315

0.1 kg/m² 0 % Sr

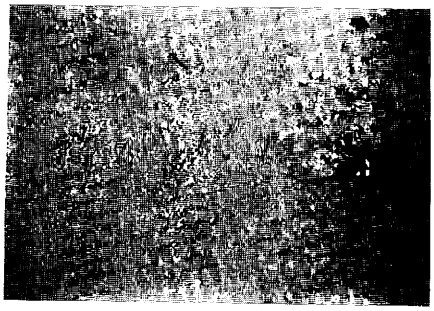

2580 FG322-1

12.8 kg/m² 1 % IDs-r, ISs-r, Ds-r

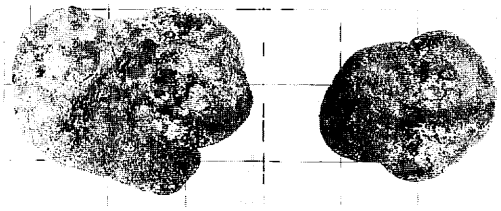

2579 P218

- - -

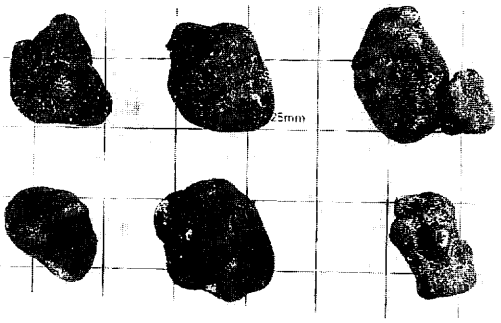

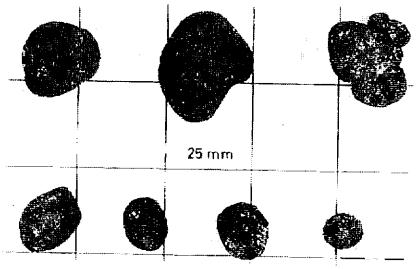

Appendix VIII-2(2)

2580 FG322-2

0.4 kg/m² 15 % IDs·r

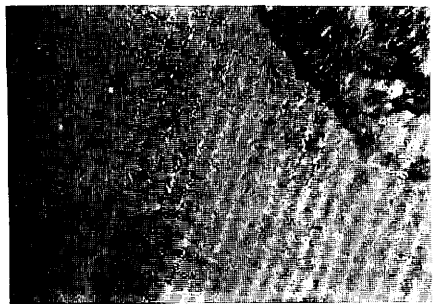

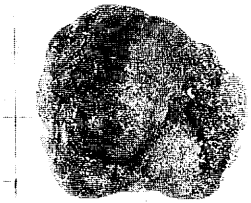

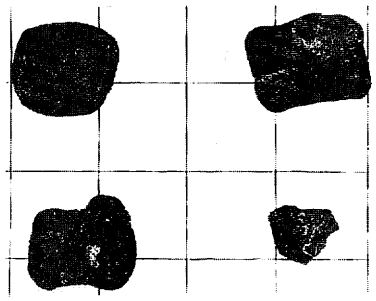

2581 FG311

0.2 kg/m² 0 % IDs·r

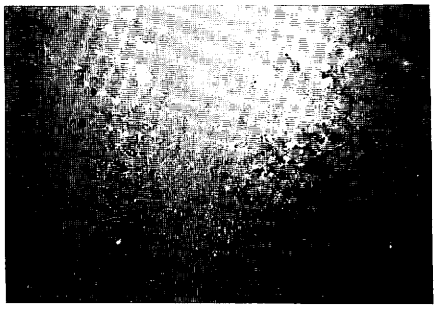

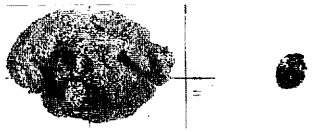

2582 FG312

0.8 kg/m² 0 % Sr

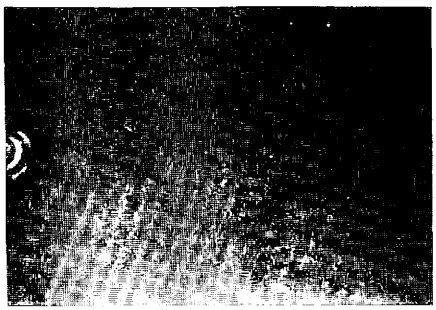

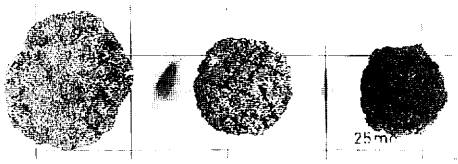

Appendix VIII-2(3)

2583 FG327

4.5 kg/m² 0 % Sr

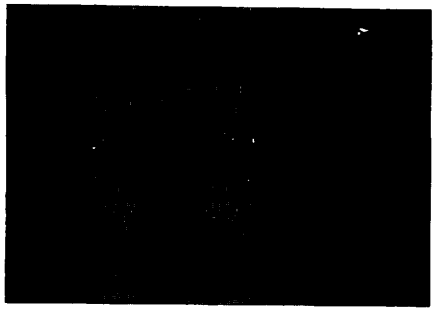

2584 FG326

0.0 kg/m² 0 % -

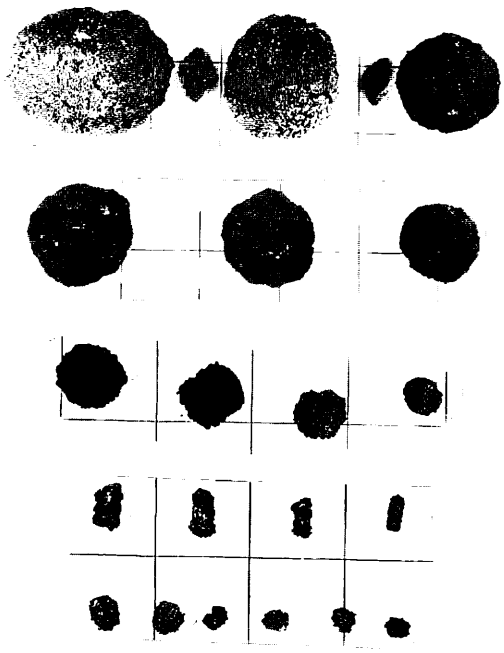

2585 FG323

0.0 kg/m² 0 % -

2586 P219

0.0 kg/m² - -

2583 P220

- - Sr

2586 FG321

- - -

Appendix VIII-2(4)

2587 FG318

0.0 kg/m² 0 % -

2589 FG324

0.0 kg/m² 0 % -

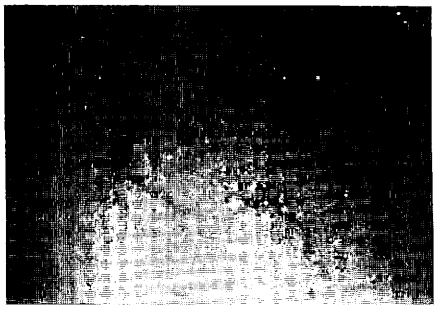

2588 FG317

0.1 kg/m² 0 % Sr

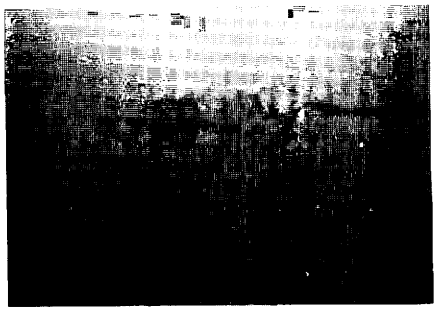

2590 FG325

0.0 kg/m² 0 % -

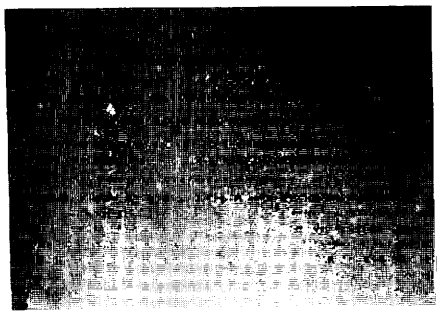

2591 P221

0.0 kg/m² - -

Appendix VIII-2(5)

2591 FG333

0.0 kg/m² 0 % –

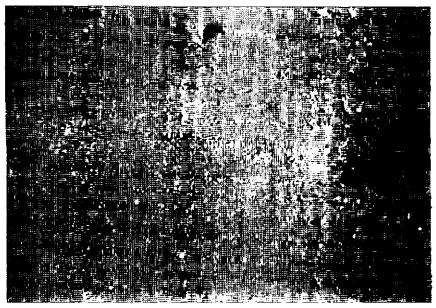

2594 FG316-1

0.1 kg/m² 0 % Sr, Dr

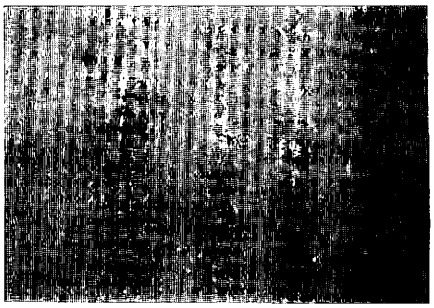

2592 FG320

0.0 kg/m² 0 % –

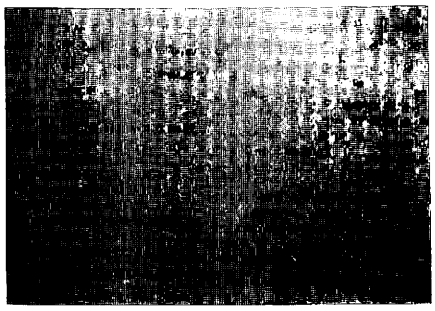

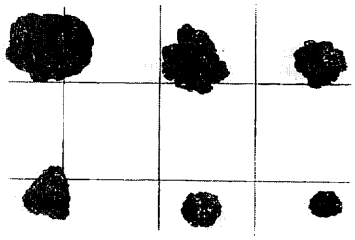

2593 FG319

0.0 kg/m² 0 % –

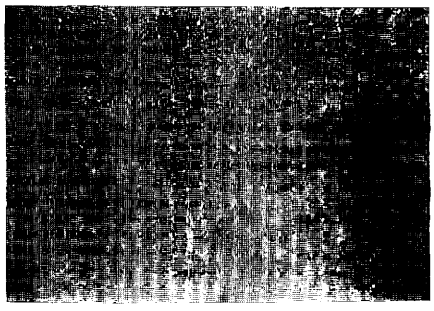

Appendix VIII-2(6)

2594 FG316-2

2.1 kg/m² 0 % IDr, IDPr

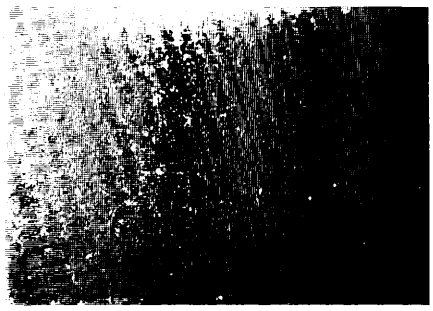

2595 FG332

0.0 kg/m² 0 % -

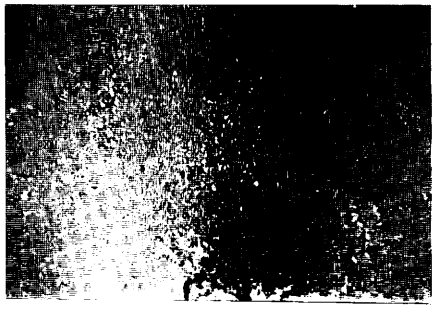

2596 FG342

0.4 kg/m² 0 % Sr

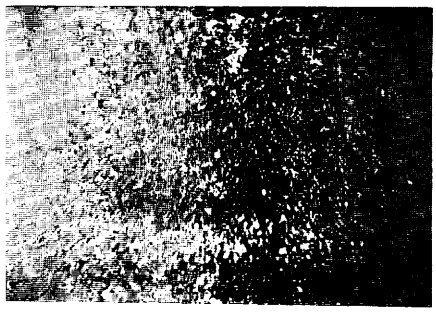

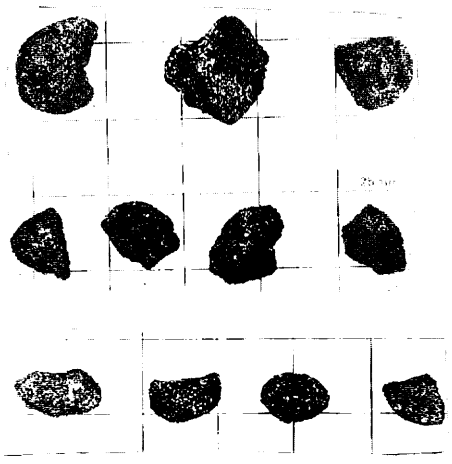

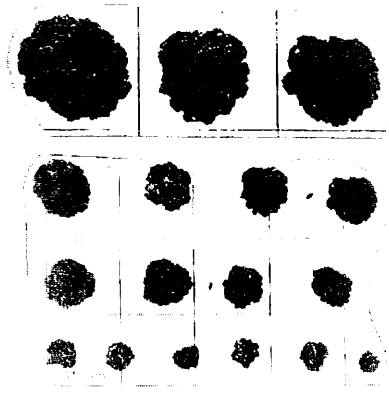

2596 P223

0.0 kg/m² - -

Appendix VIII-2(7)

2599 FG328-2

0.0 kg/m² 0 % -

2602 FG330

0.0 kg/m² 0 % -

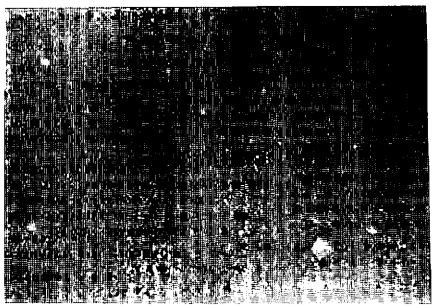

2600 P222

0.0 kg/m² - -

2600 FG340

0.0 kg/m² 0 % -

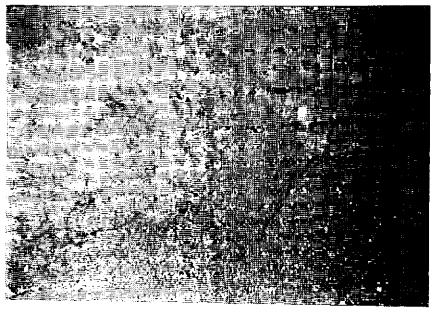

2603 FG331

0.0 kg/m² 0 % -

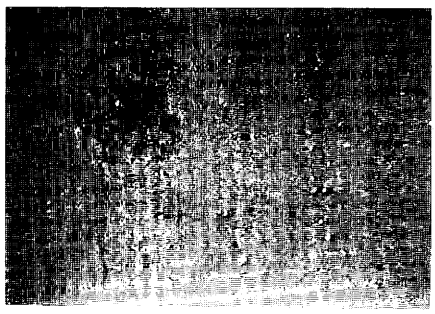

2601 FG339

0.0 kg/m² 0 % -

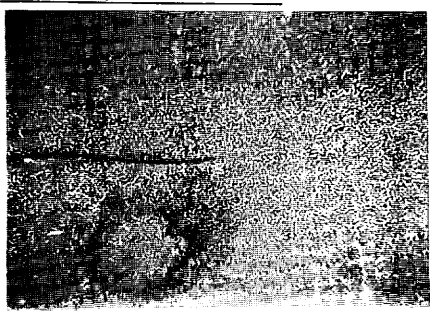

2604 FG336

0.0 kg/m² 0 % -

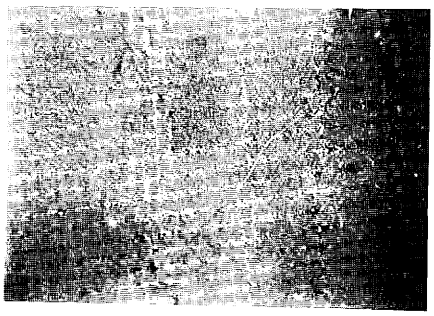

Appendix VIII-2(8)

2605 FG335

12.6 kg/m² 0 % DPs·r, Ts·r, Fs·r, Ds·r

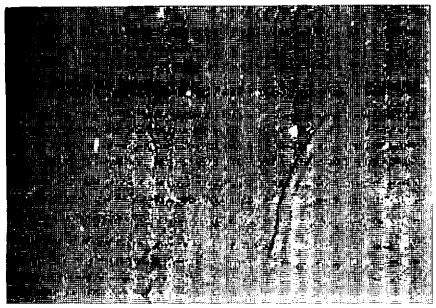

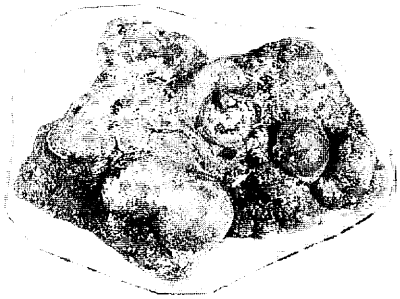

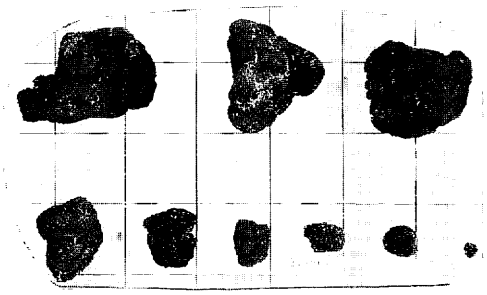

2606 FG334

0.3 kg/m² 0 % Sr

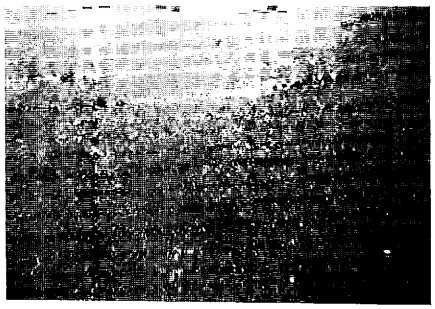

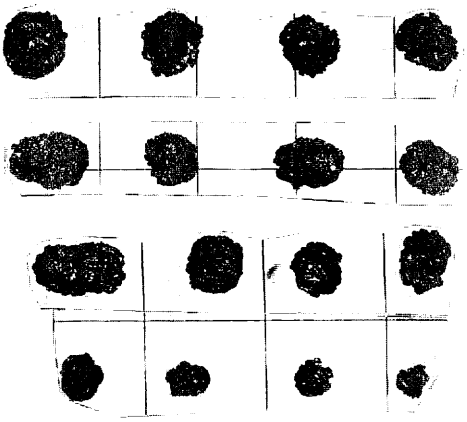

2607 FG337

0.0 kg/m² 0 % -

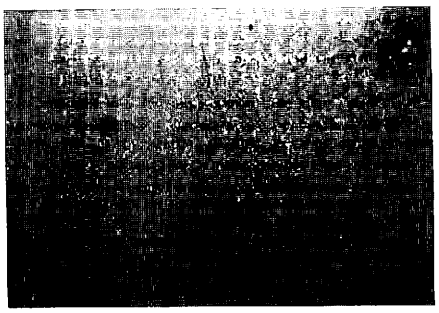

Appendix VIII-2(9)

2597 FG341-1

0.3 kg/m² 0 % Sr

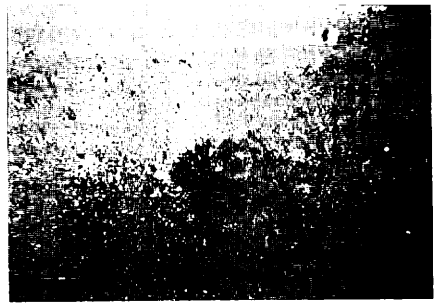

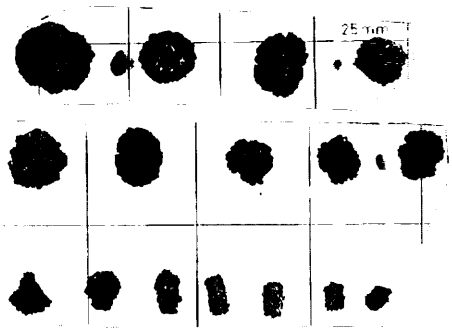

2598 FG329

0.8 kg/m² 0 % Sr

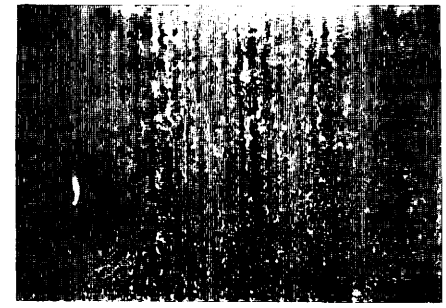

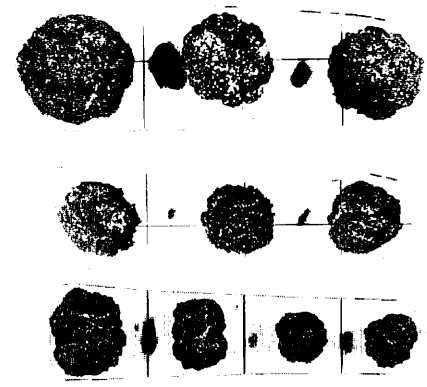

2597 FG341-2

0.1 kg/m² 0 % Sr

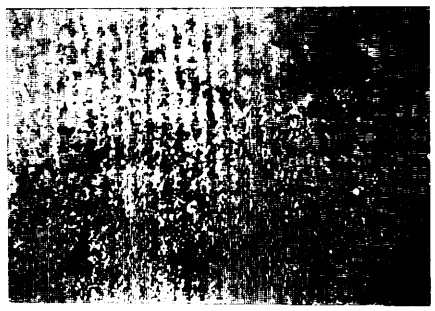

2599 FG328-1

0.0 kg/m² 0 % -

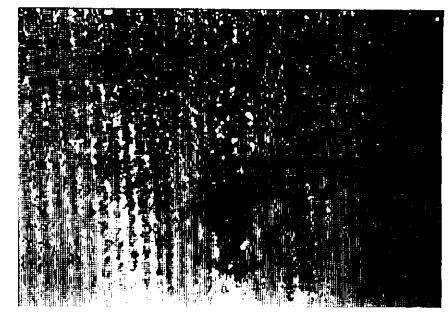

Appendix VIII-2(10)

AREA I

2608 FG338

4.9 kg/m² 0 % Sr

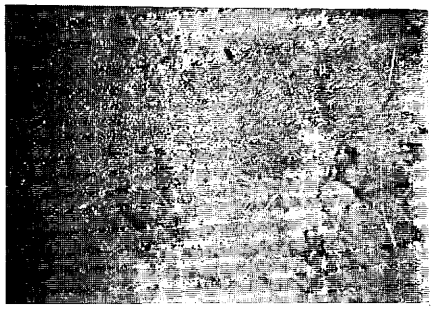

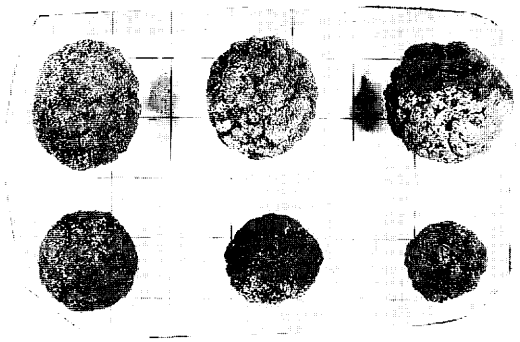

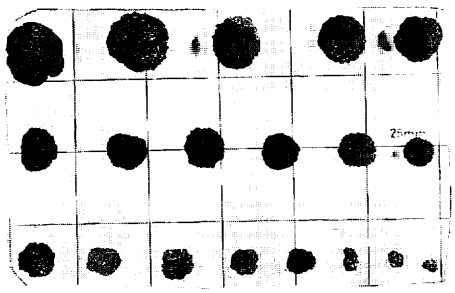

2609 FG343

1.3 kg/m² 0 % Sr

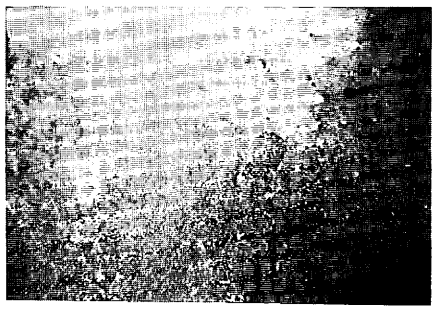

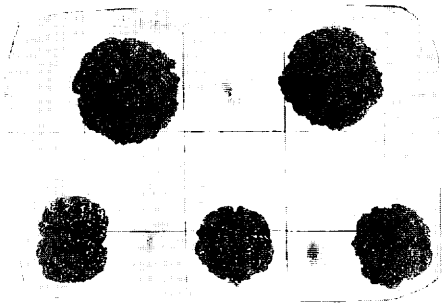

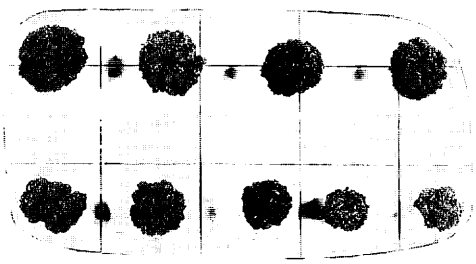

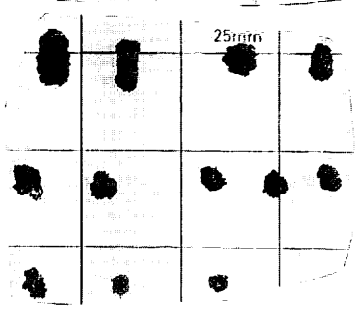

Appendix VIII-2(11)

2610 FG344

0.1 kg/m² 0 % Sr

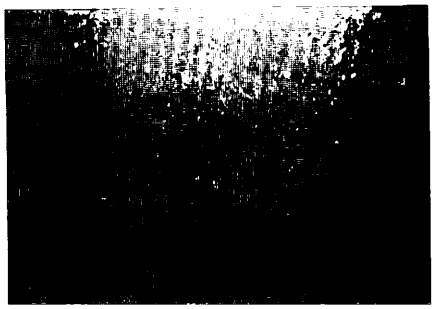

2612 FG346

0.0 kg/m² 0 % -

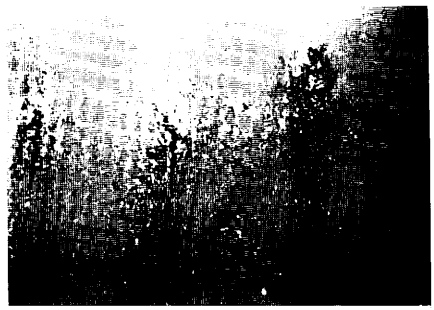

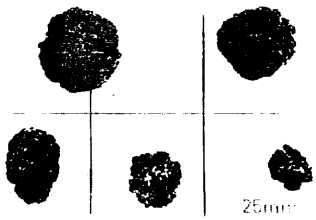

2613 B57

0.1 kg/m² 0 % Vr

box core surface

2611 FG345

0.1 kg/m² 0 % Sr

Appendix VIII-2(12)

2614 FG347

0.1 kg/m² 0 % Vr

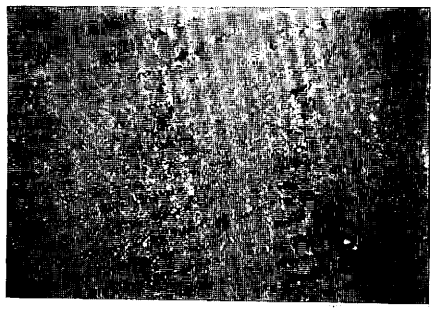

2617 FG350

0.1 kg/m² 0 % (Dr)

2615 FG348

0.0 kg/m² 0 % -

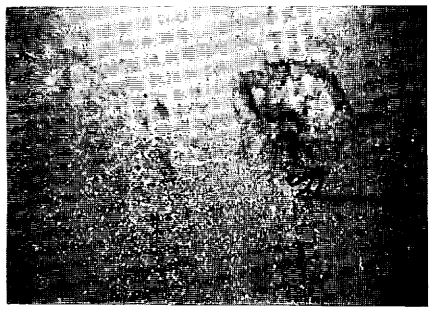

2618 B58

0.1 kg/m² 0 % Sr

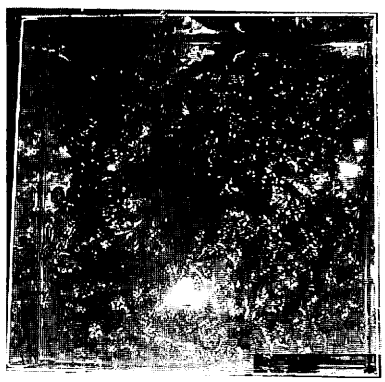

box core surface

2616 FG349

0.0 kg/m² 0 % -

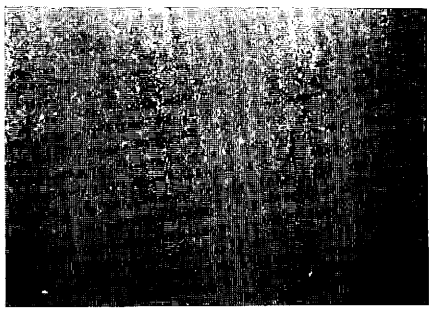

Appendix VIII-2(13)

2619 FG351

2.8 kg/m² 1 % Sr,Dr

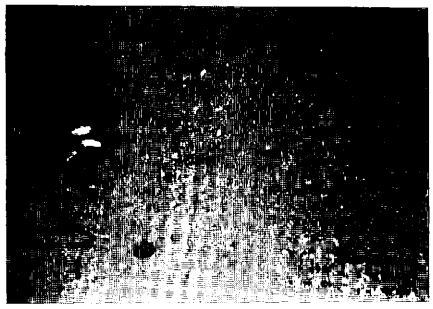

2620 FG352

9.6 kg/m² 0 % Sr,Dr

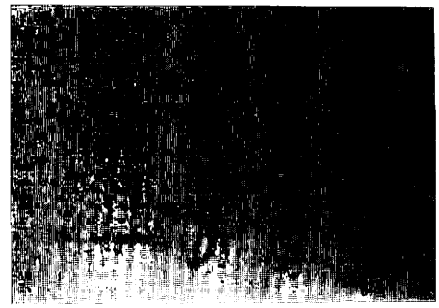

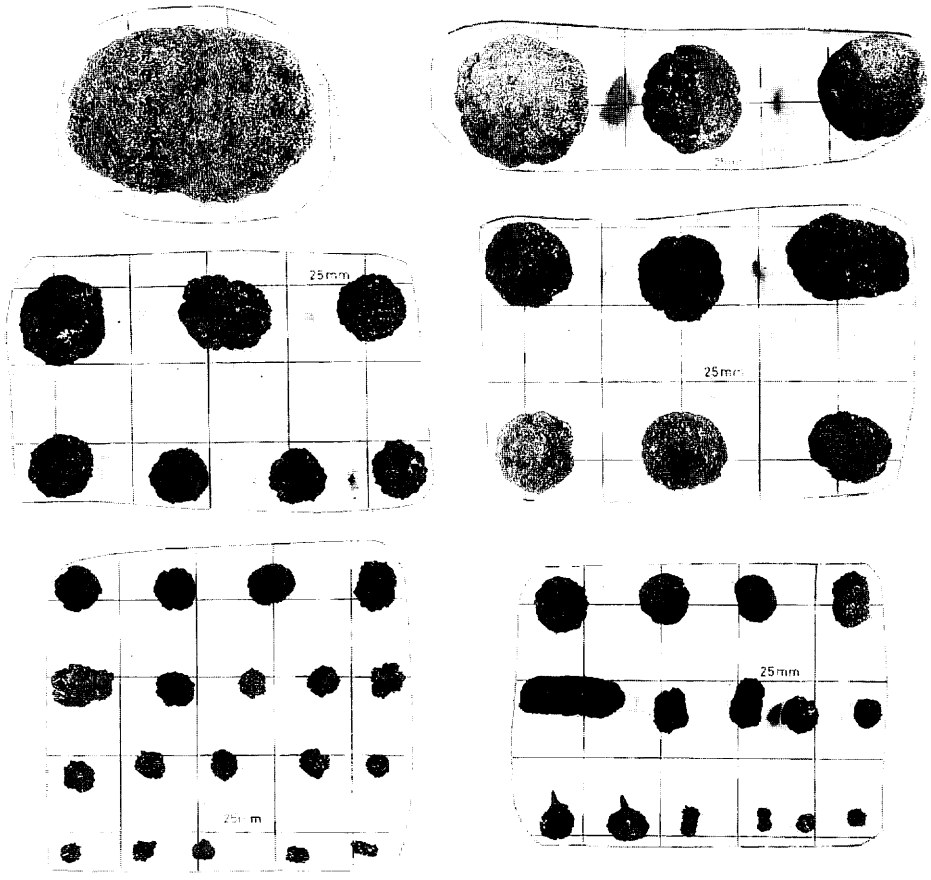

Appendix VIII-2(14)

2621 FG353

15.6 kg/m² 30 % ISPs, IDPs, IDs, Is

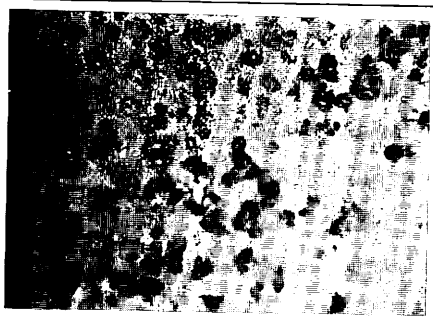

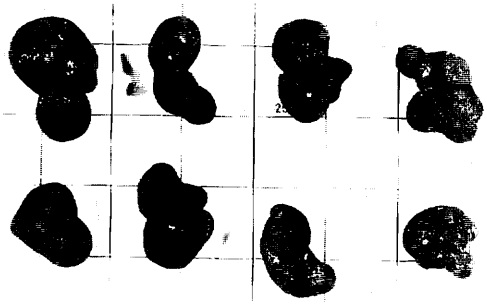

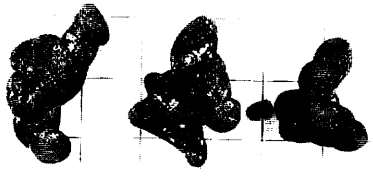

2622 B59

15.7 kg/m² 30 % IDPs, DPs

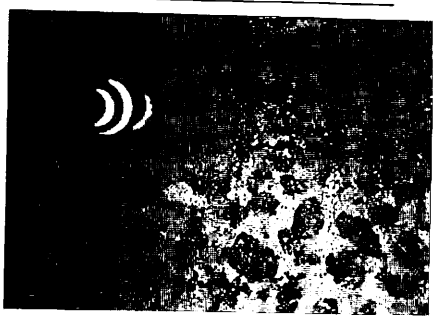

box core surface

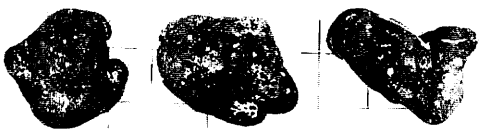

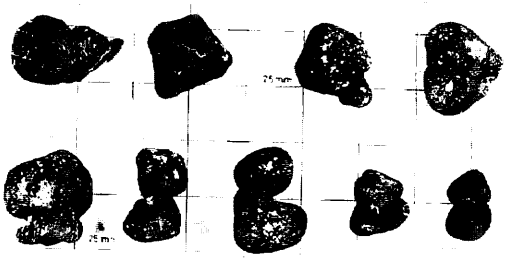

Appendix VIII-2(15)

2623 FG354

0.0 kg/m² 40 % –

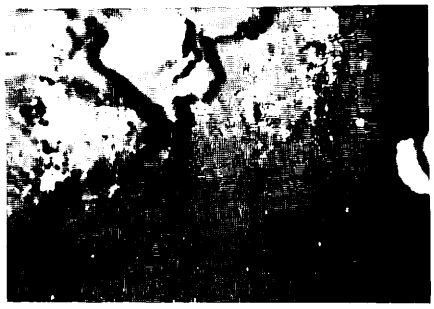

2625 FG356

11.4 kg/m² 2 % Sr,Dr

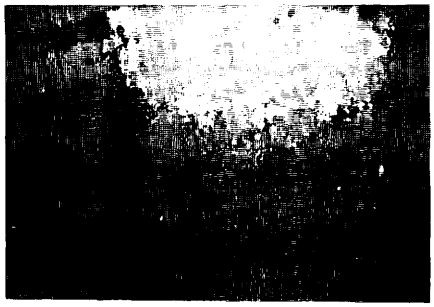

2624 FG355

5.2 kg/m² 0 % Sr,Dr

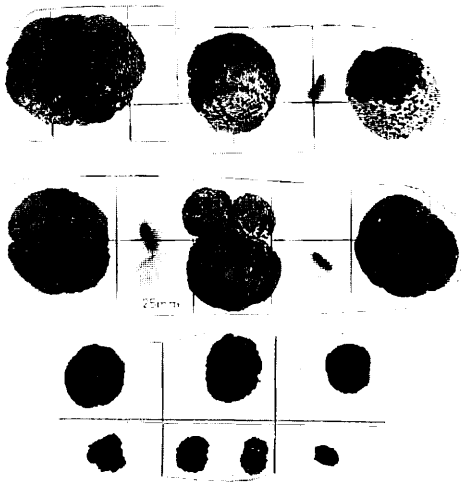

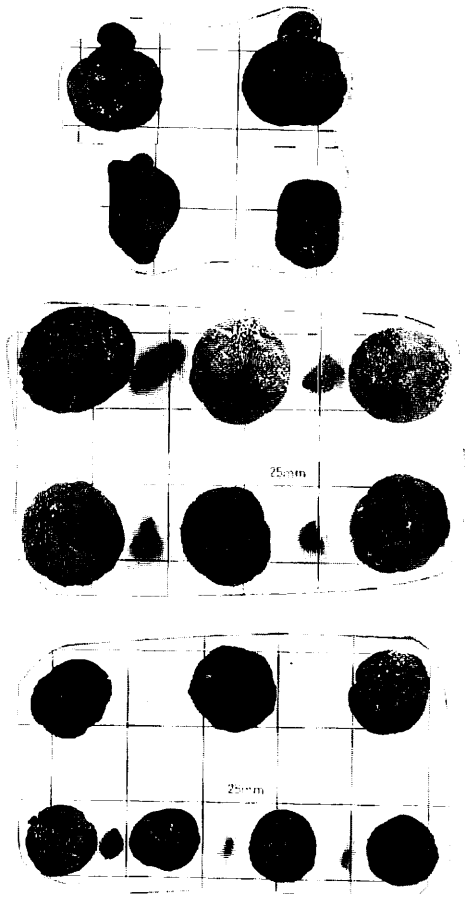

Appendix VIII-2(16)

2626 FG357

5.9 kg/m² - Sr

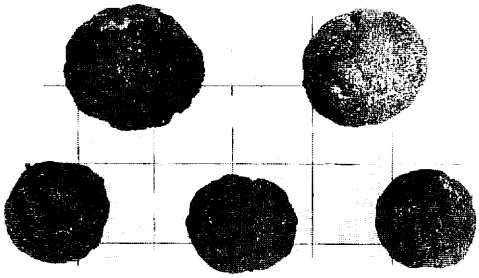

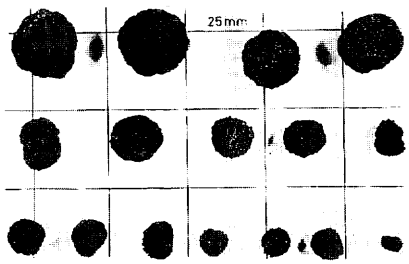

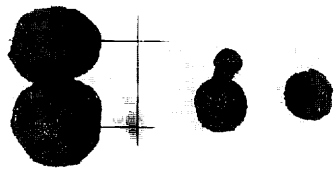

2627 FG358

5.8 kg/m² 1 % Sr

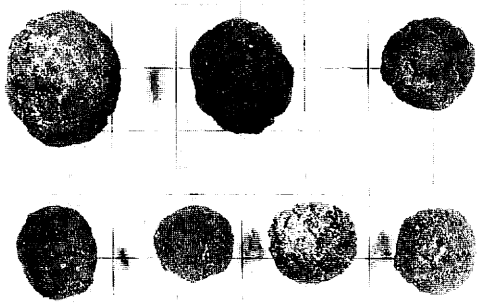

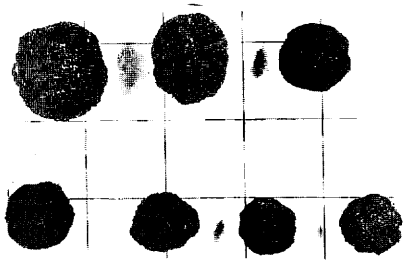

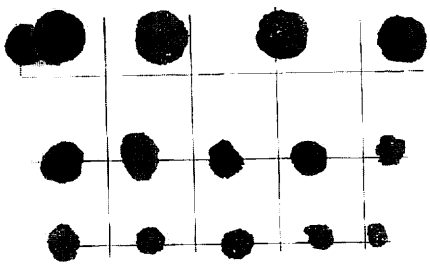

Appendix VIII-2(17)

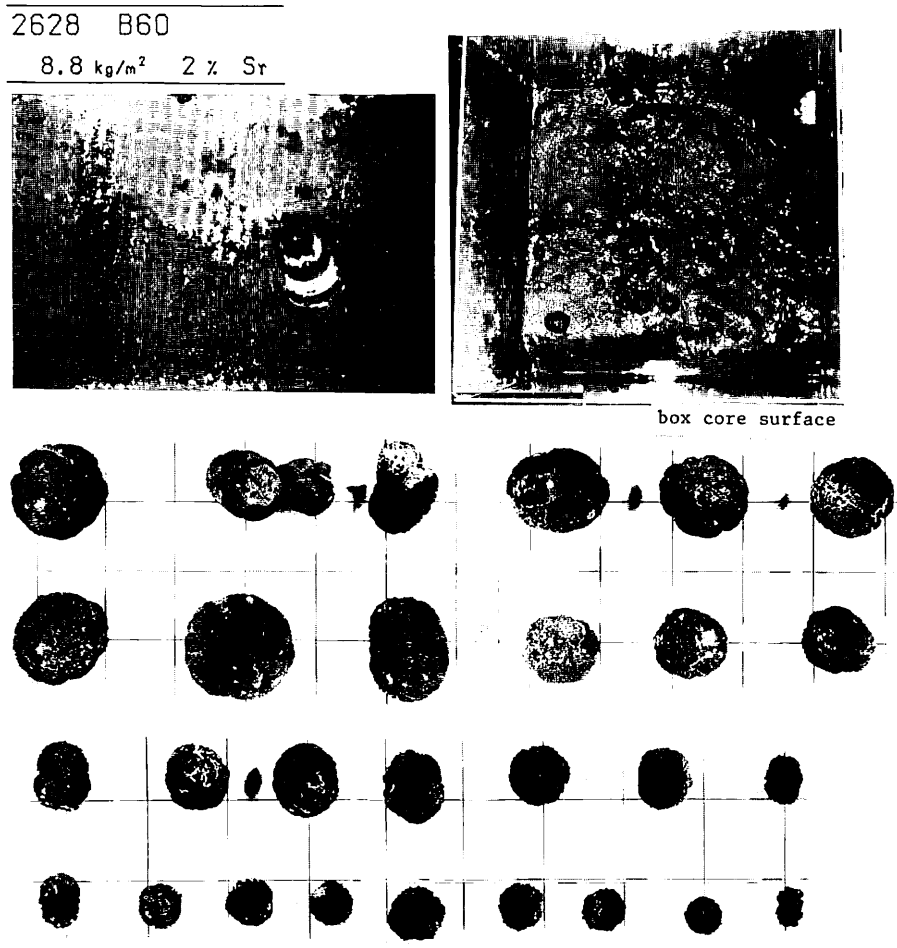

Appendix VIII-2(18)

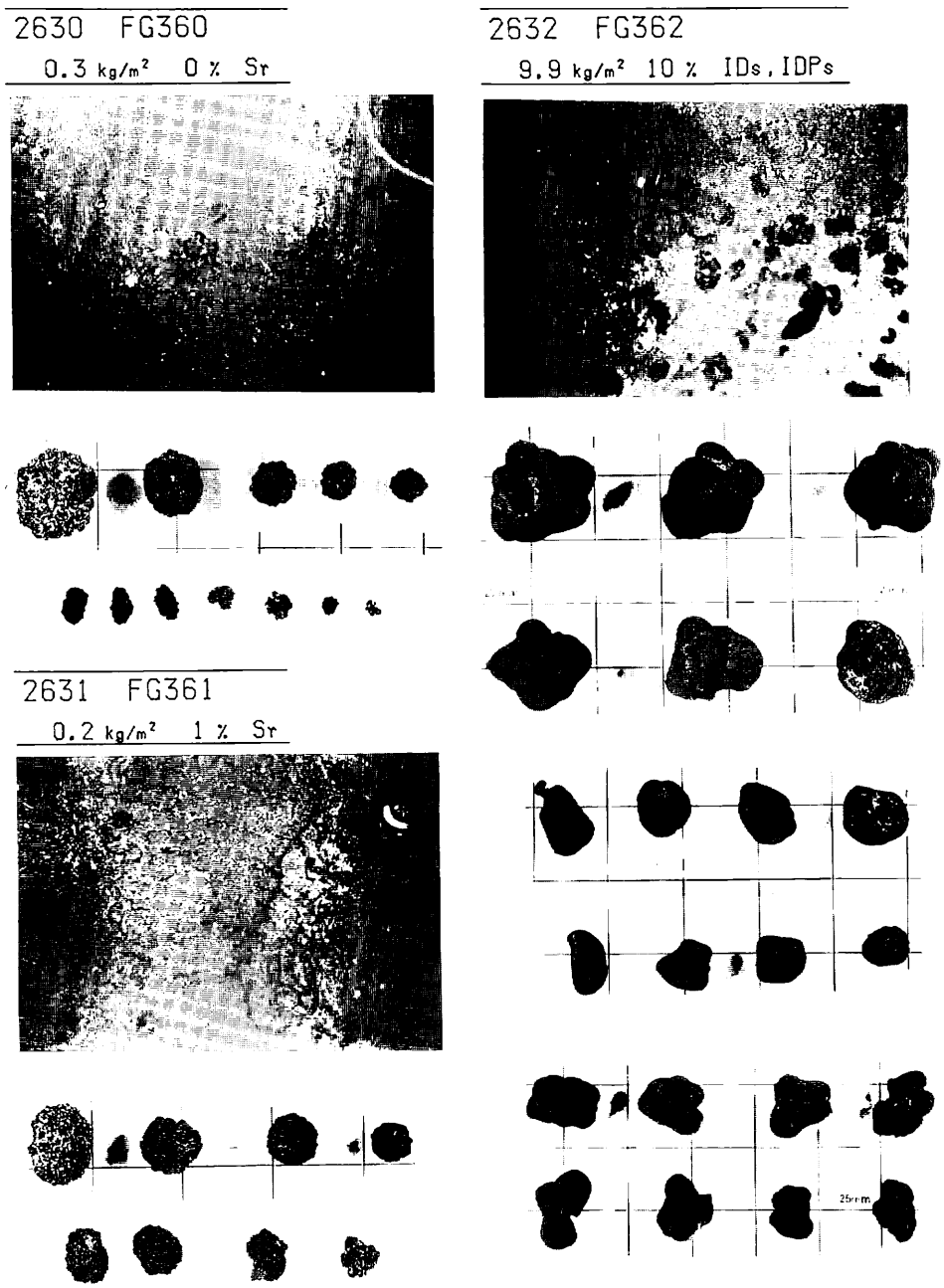

Appendix VIII-2(19)

2633 FG363

15.1 kg/m² 25 % IDs, IDPs

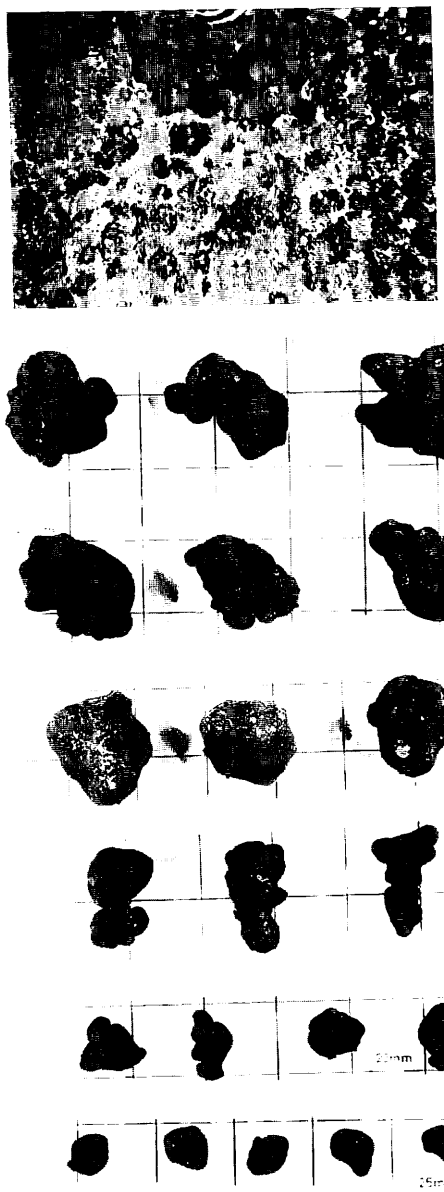

2634 B61

14.6 kg/m² 40 % IDs, IDPs, Fs

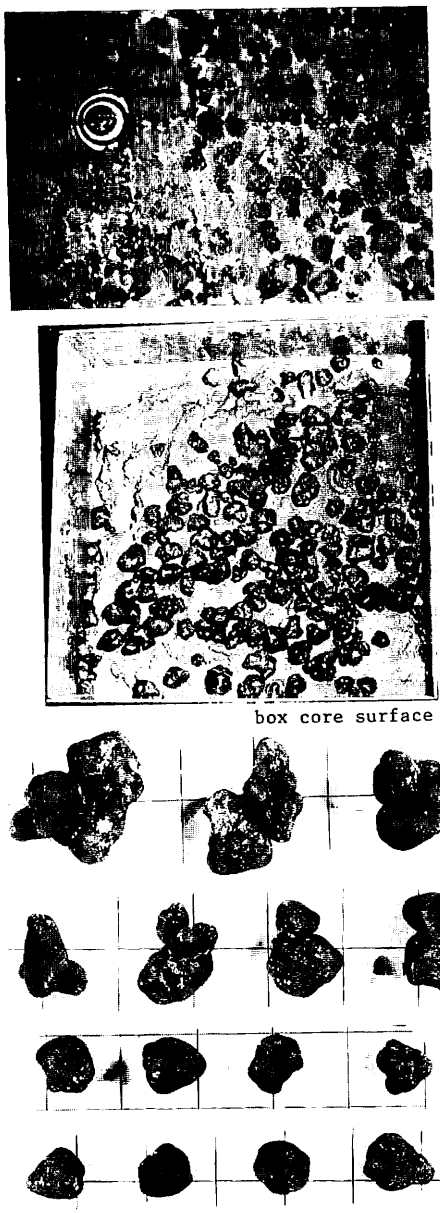

box core surface

Appendix VIII-2(20)

2635 FG364

10.2 kg/m² 15 % IDs, IDPs, Is

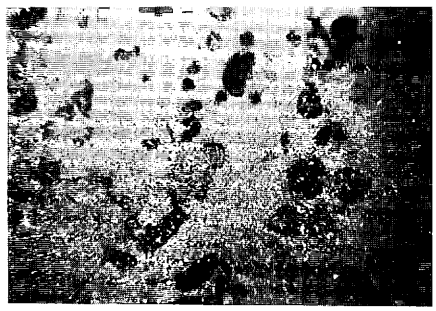

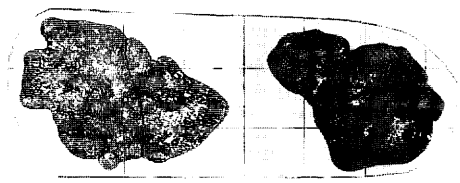

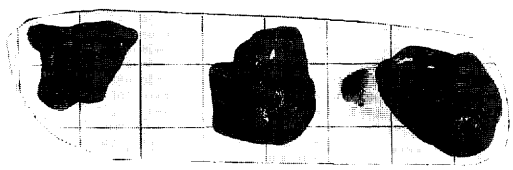

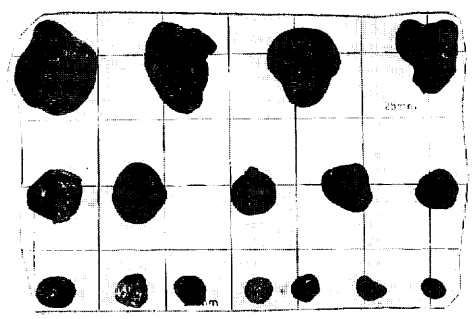

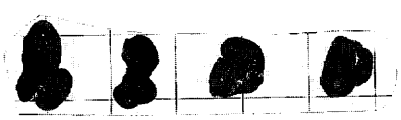

2636 FG365

3.0 kg/m² 0 % Sr

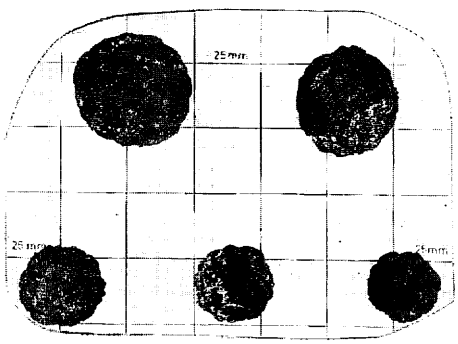

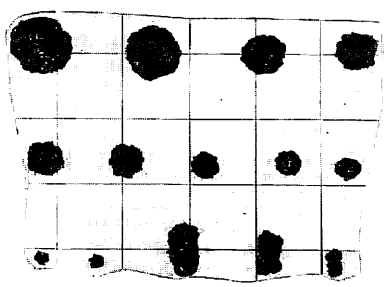

Appendix VIII-2(21)

2637 FG366

0.6 kg/m² 0 % Sr

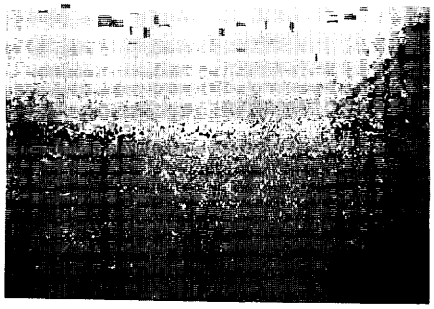

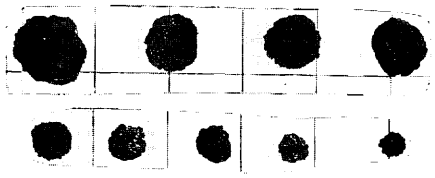

2638 FG367

1.3 kg/m² 0 % Sr

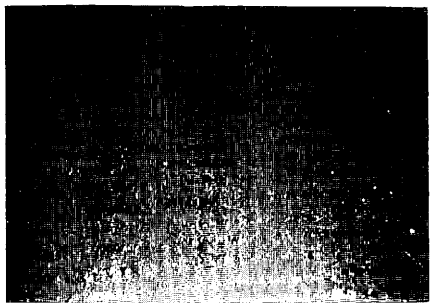

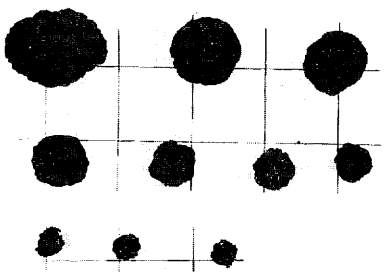

2640 FG368

14.8 kg/m² 15 % Ds,DPs,IDs

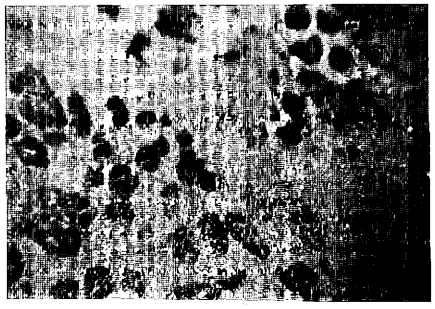

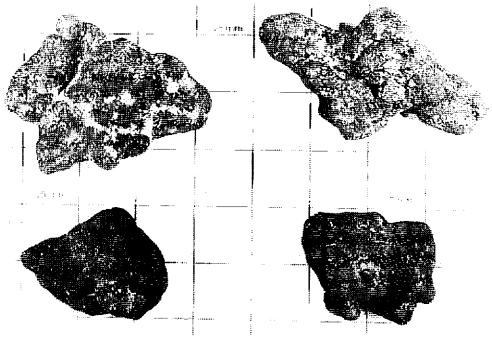

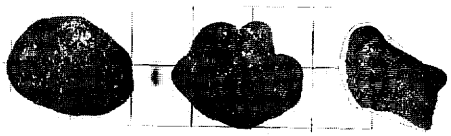

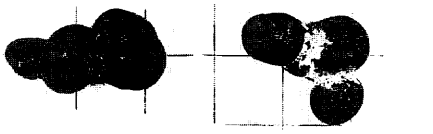

Appendix VIII-2(22)

2641 FG369

1.7 kg/m² 0 % Sr

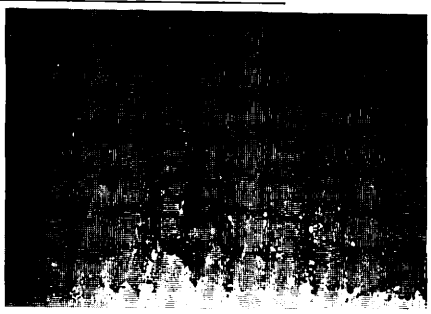

2642 FG370

0.2 kg/m² 0 % Sr

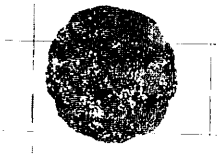

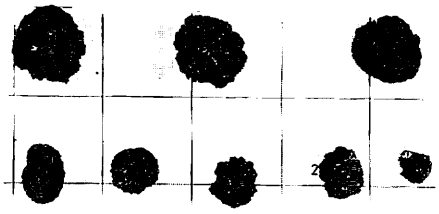

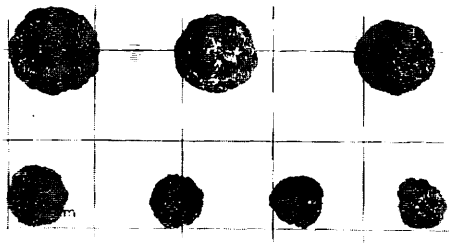

2643 FG371

0.0 kg/m² 0 % -

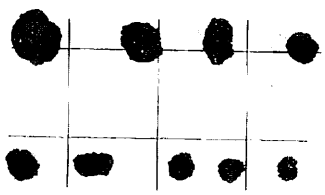

Appendix VIII-2(23)

2644 FG372

0.1 kg/m² 0 % Sr

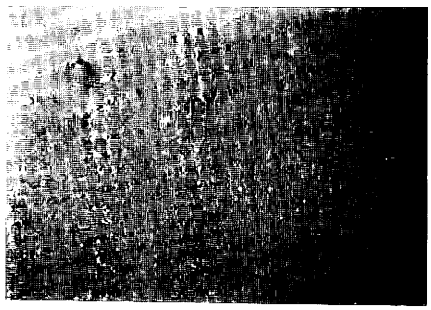

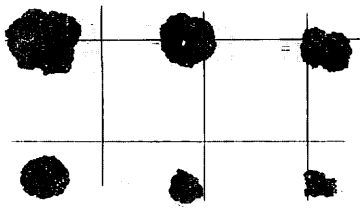

2646 FG373

4.9 kg/m² 2 % IDr, IDPr, Fr

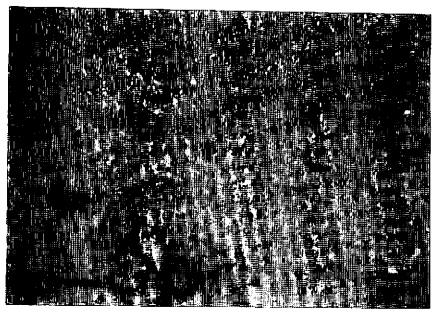

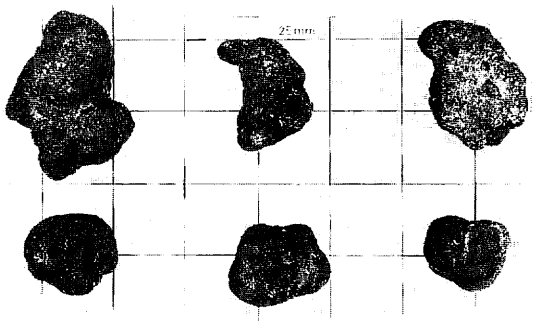

2645 B63

(12.0 kg/m²) 0 % -

nodules at 15 cm depth

see Appendix -3

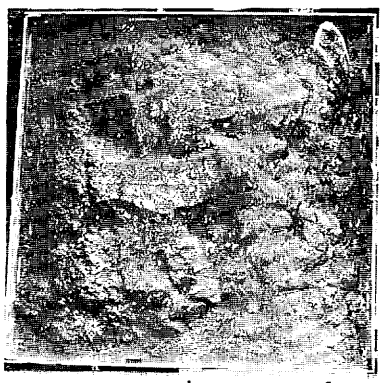

box core surface

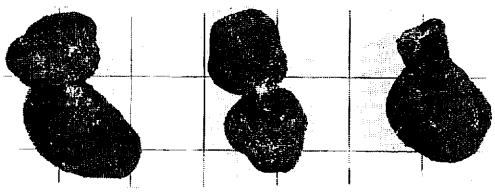

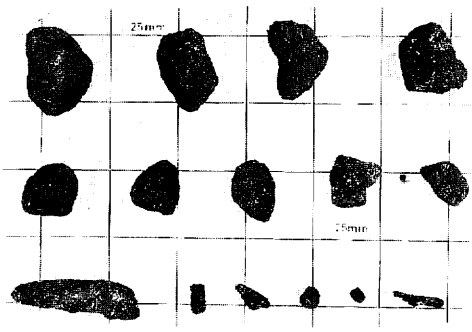

2647 FG374

0.0 kg/m² - (IDr)

2648 FG375

10.2 kg/m² 5 % Sr,Dr

2649 FG376

10.4 kg/m² 15 % Sr,Dr

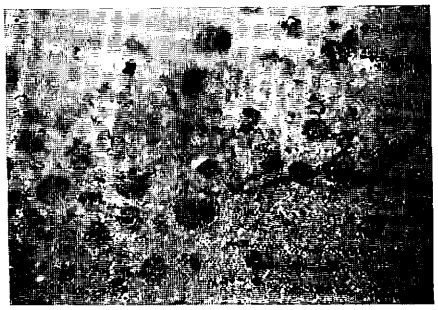

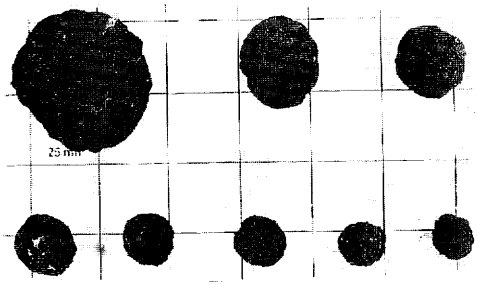

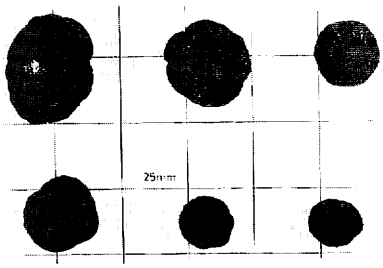

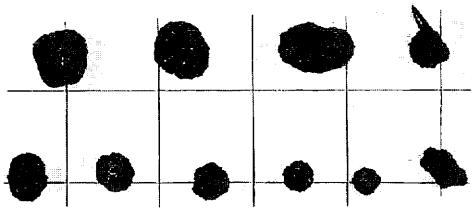

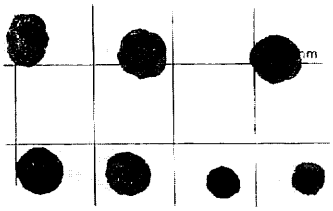

Appendix VIII-2(25)

2650 FG377

8.1 kg/m² 10 % IDs·r, Ss·r, Ts·r

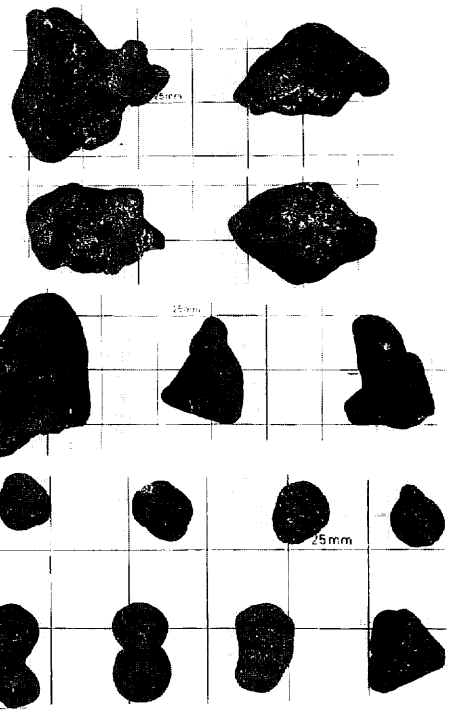

2652 FG378

9.5 kg/m² 30 % IDs, IDPs

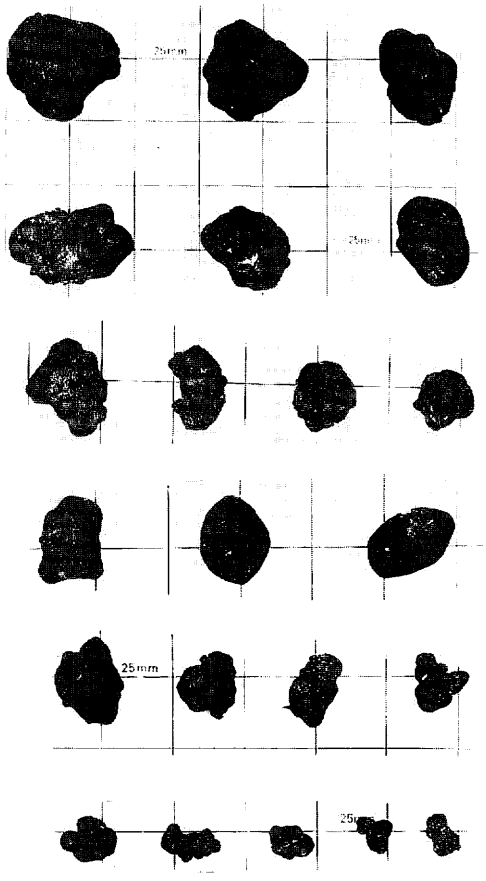

2651 P224

– – Ss

Appendix VIII-2(26)

2653 FG379

4.0 kg/m² 2 % IDs

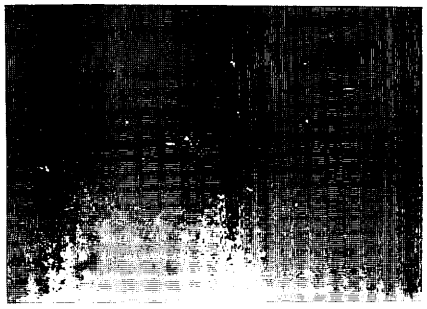

2654 FG380

15.1 kg/m², 10 % IDs, IDPs

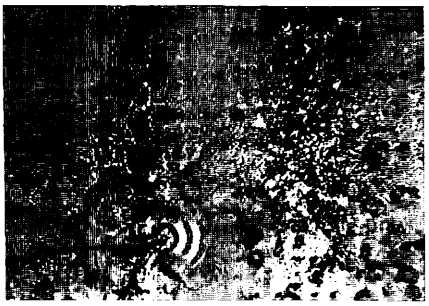

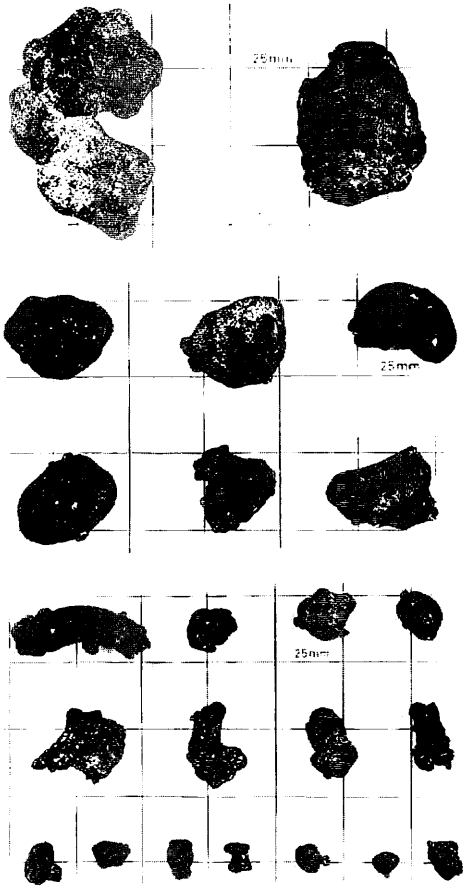

2655 FG381

18.0 kg/m² 10 % Ss·r, Ds·r, Fs·r, IDs·r

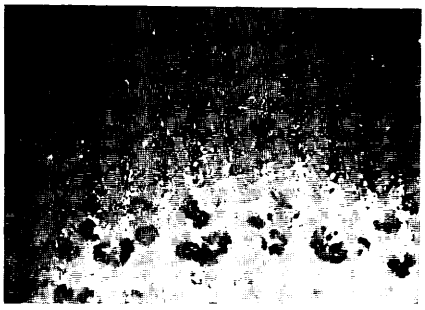

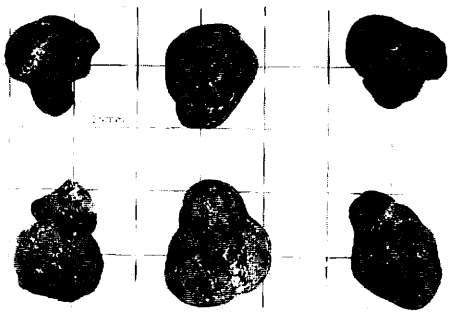

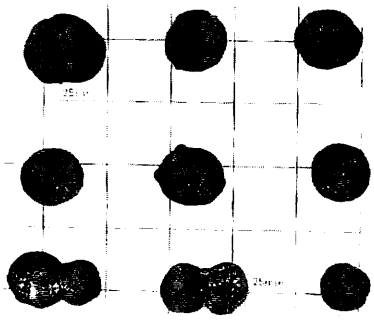

2656 FG382

0.5 kg/m² 0 % Sr

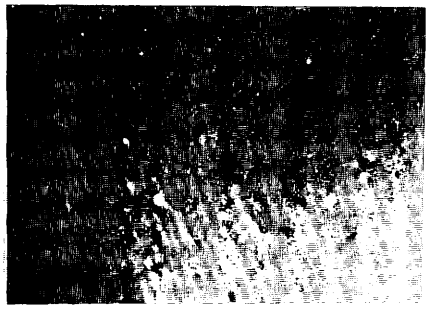

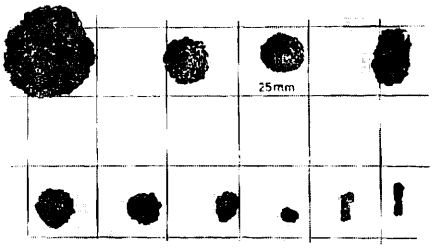

Appendix VIII-2(28)

2657 B64

1.1 kg/m² 0 % Sr

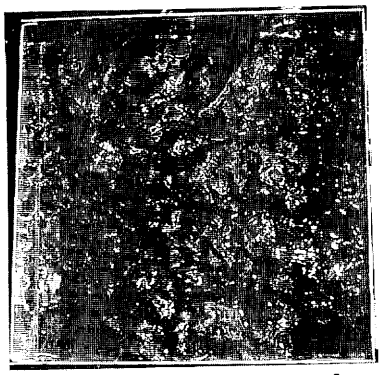

box core surface

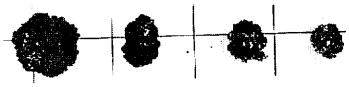

2658 FG383

0.0 kg/m² 0 % Vs

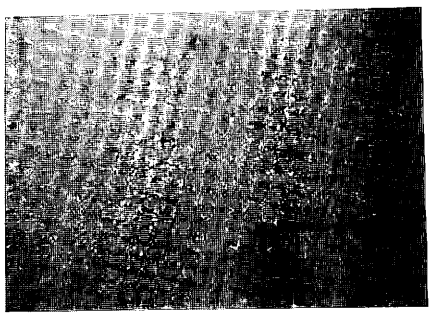

2659 FG384

8.9 kg/m² 20 % IDs, Ts

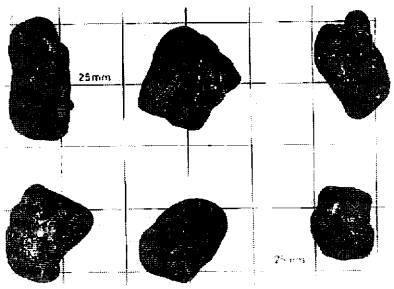

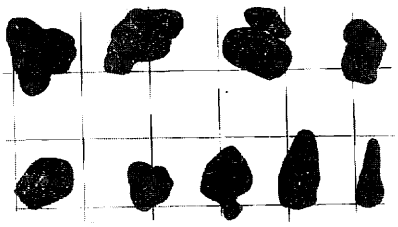

2660 FG385

13.0 kg/m² 10 % IDs, ISs, Vs

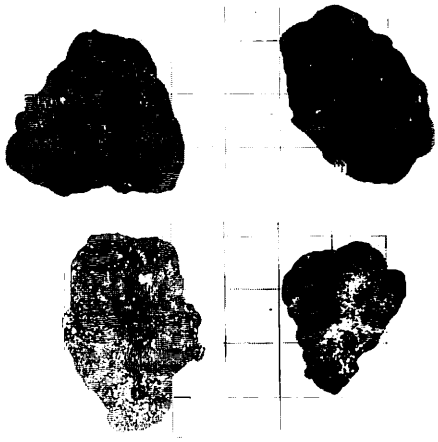

2661 FG386

10.5 kg/m² - Ss·r, Ds·r

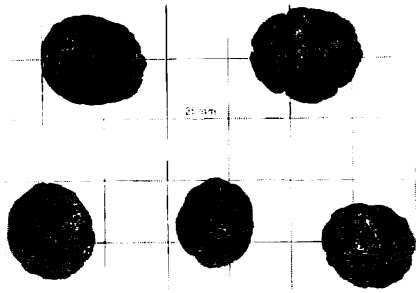

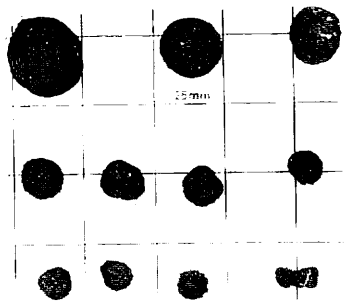

2662 FG387

0.8 kg/m² - Sr

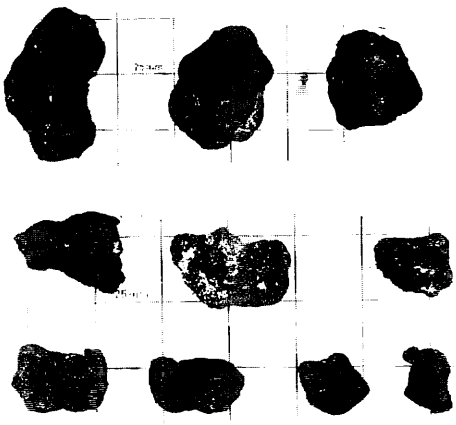

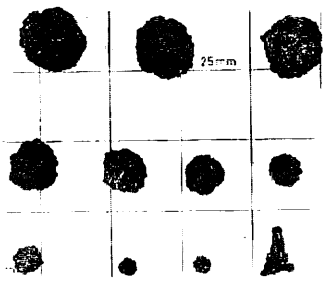

Appendix VIII-2(30)

2663 P225

– – Dsr

2664 FG388

0.0 kg/m² 0 % Vs

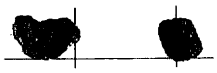

2665 FG389

0.0 kg/m² 0 % –

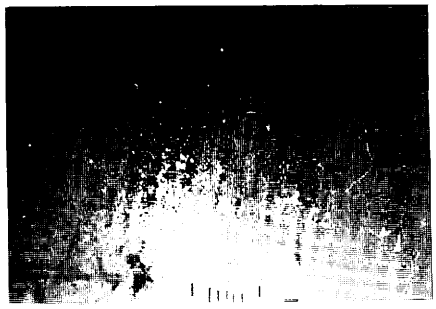

2666 FG390

0.0 kg/m² 0 % Dr

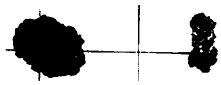

2667 FG391

0.3 kg/m² 0 % Sr

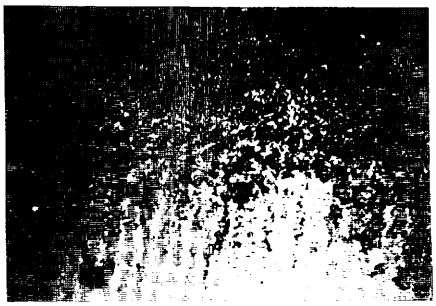

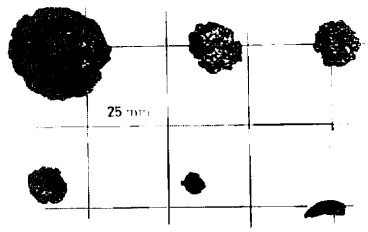

2668 FG392

0.9 kg/m² 0 % Sr

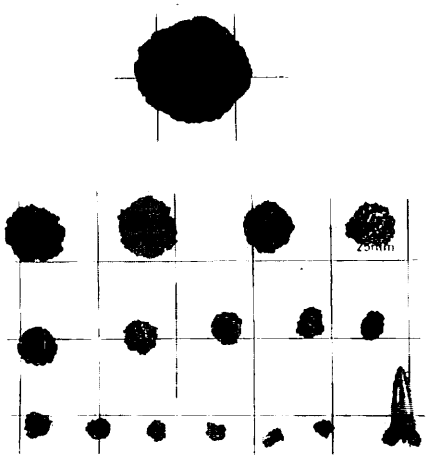

2669 B65

0.4 kg/m² 0 % Sr

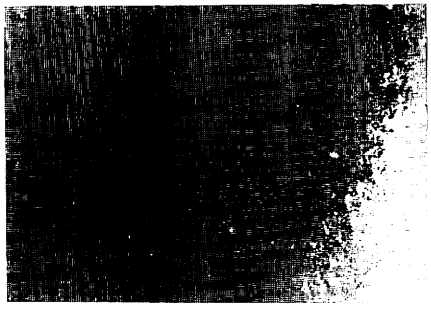

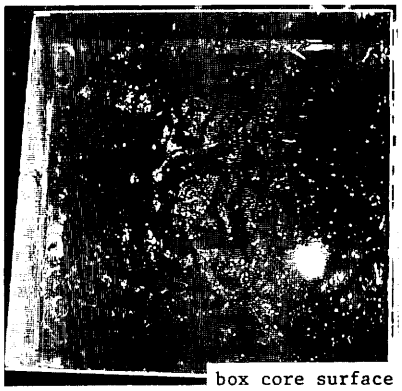

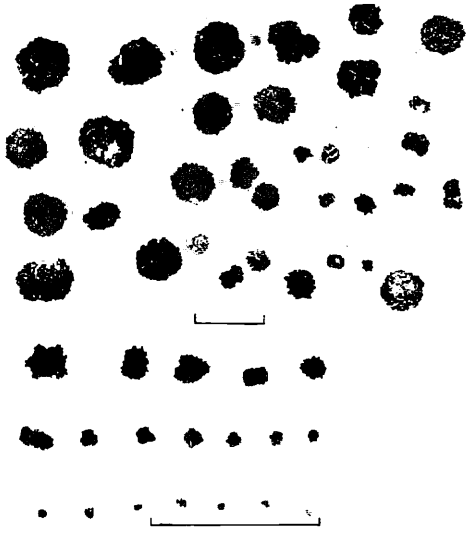

Appendix VIII-2(32)

2670 FG424

3.3 kg/m² 0 % Sr

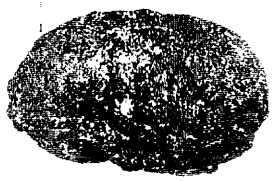

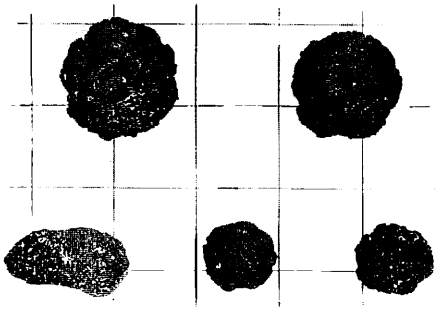

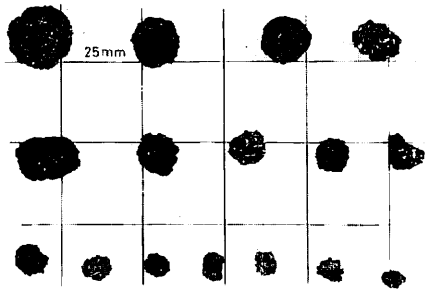

2671 FG425

0.0 kg/m² - Dr

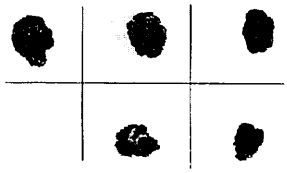

2672 FG426

0.0 kg/m² 0 % Fr

2673 FG427

0.0 kg/m² - Vr

Appendix VIII-2(33)

AREA II

2674 FG428

0.0 kg/m² 0 % –

2675 P230

0.0 kg/m² – –

2676 P226

0.0 kg/m² – –

2676 FG393-1

0.0 kg/m² 0 % –

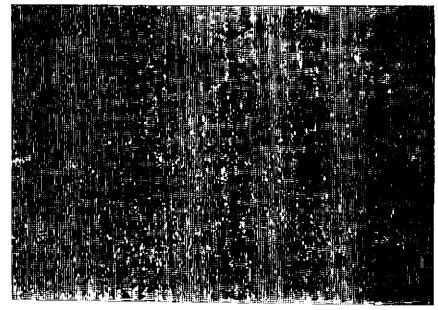

2676 FG393-2

0.0 kg/m² 0 % –

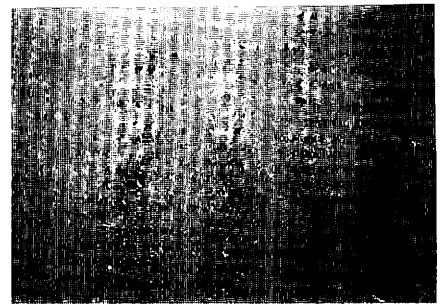

2677 FG394

0.4 kg/m² 0 % Sr

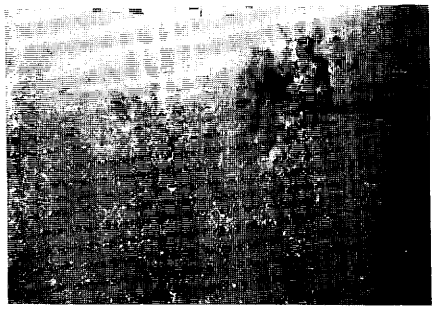

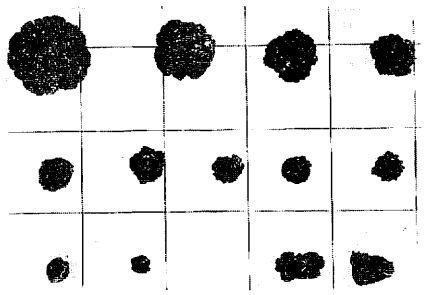

2679 FG396

0.1 kg/m² 0 % Sr

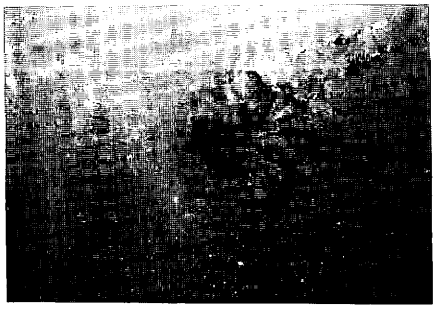

2678 FG395

0.1 kg/m² – Sr

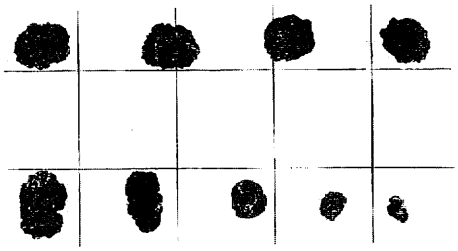

2680 FG397

0.1 kg/m² 0 % Sr

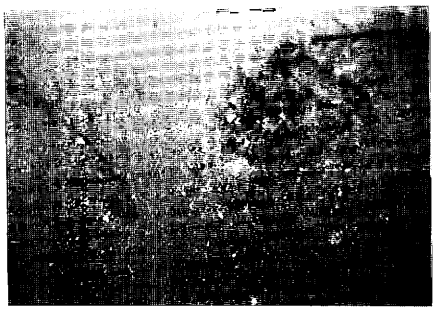

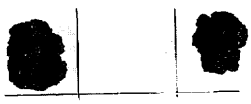

2681 B66

0.1 kg/m² 0 % Sr

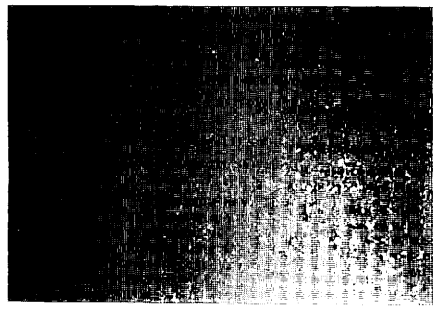

box core surface

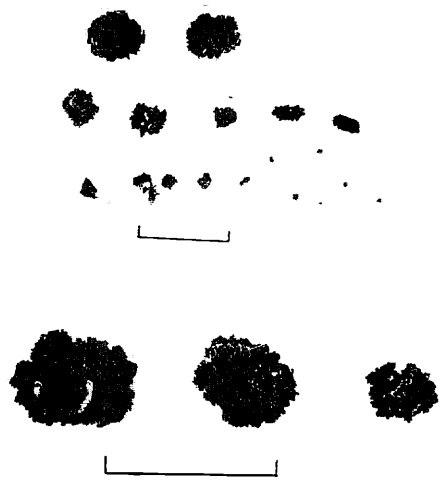

2682 FG398

0.0 kg/m² 0 % -

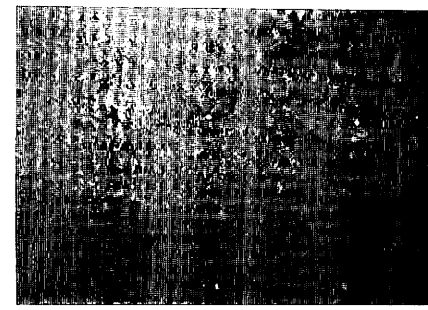

2683 FG399

0.0 kg/m² 0 % -

2684 FG400

0.0 kg/m² 0 % Sr

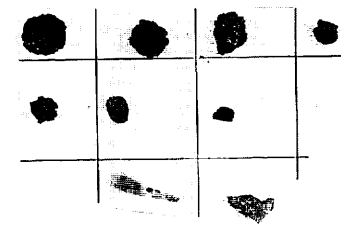

2685 FG401

0.0 kg/m² - -

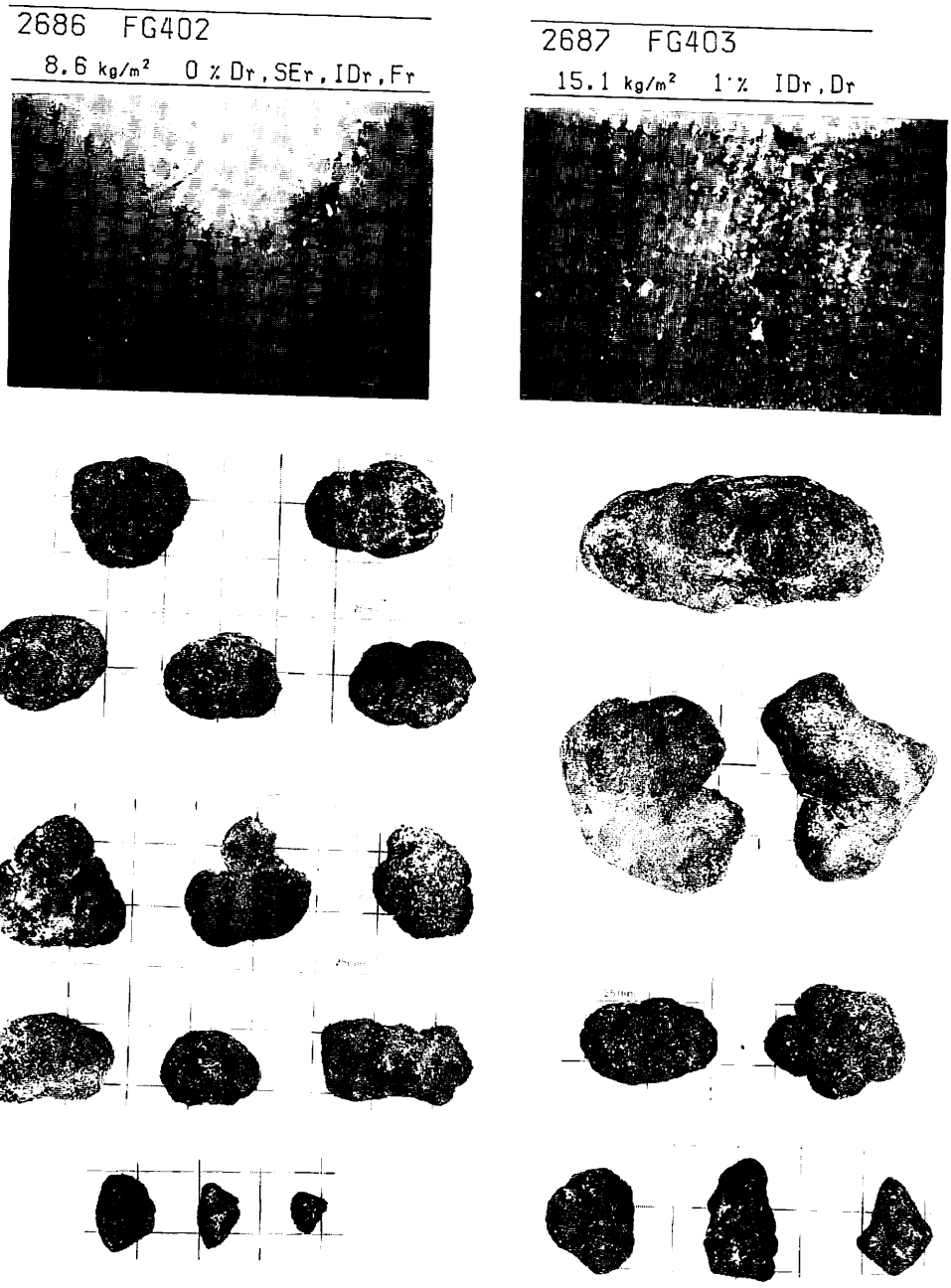

Appendix VIII-2(37)

2688 P227

0.0 kg/m² - -

2689 FG404

0.0 kg/m² 0 % -

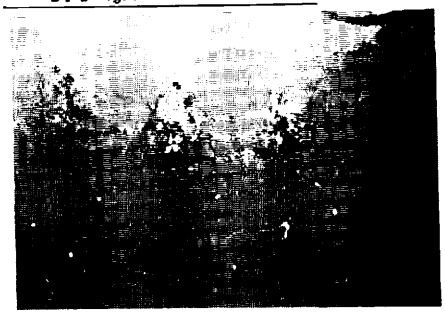

2690 FG405

0.0 kg/m² 0 % Sr

2691 FG406

0.0 kg/m² 0 % -

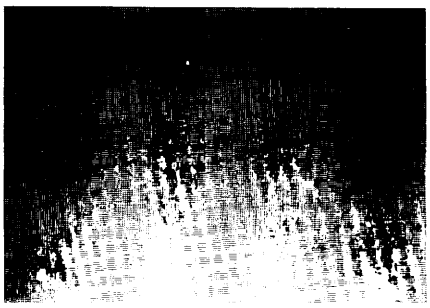

2692 FG407

7.6 kg/m² 5 % IDs-r, Fs-r

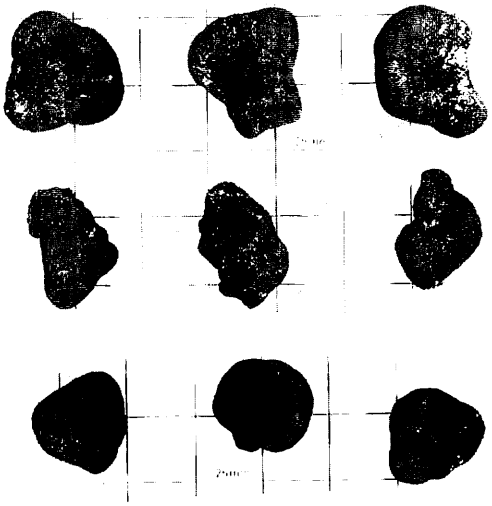

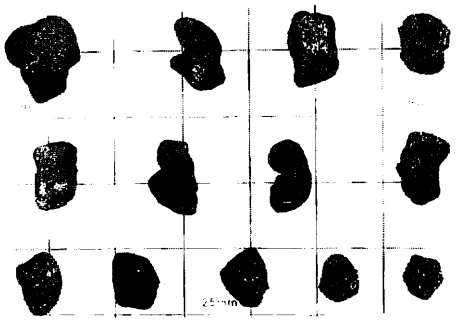

Appendix VIII-2(38)

2693 FG408

5.7 kg/m² - Sr,Fr,Dr

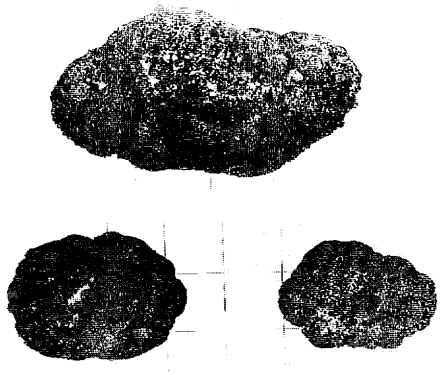

2695 B67

3.3 kg/m² 2 % IDr,Fr

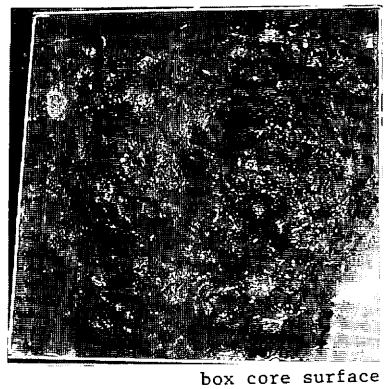

box core surface

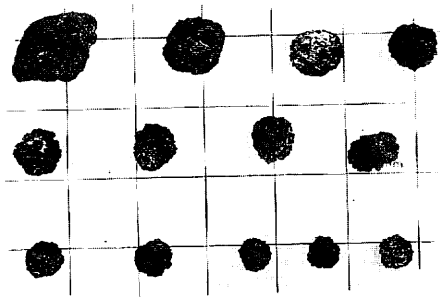

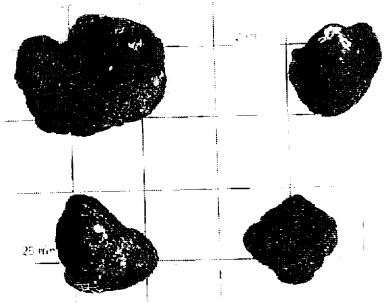

2694 FG409

0.0 kg/m² 0 % -

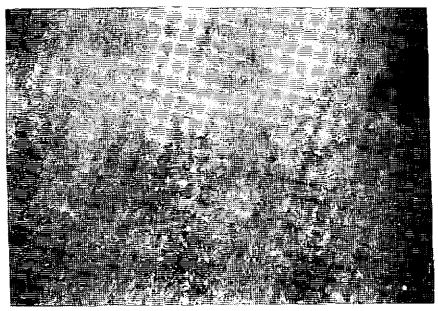

Appendix VIII-2(39)

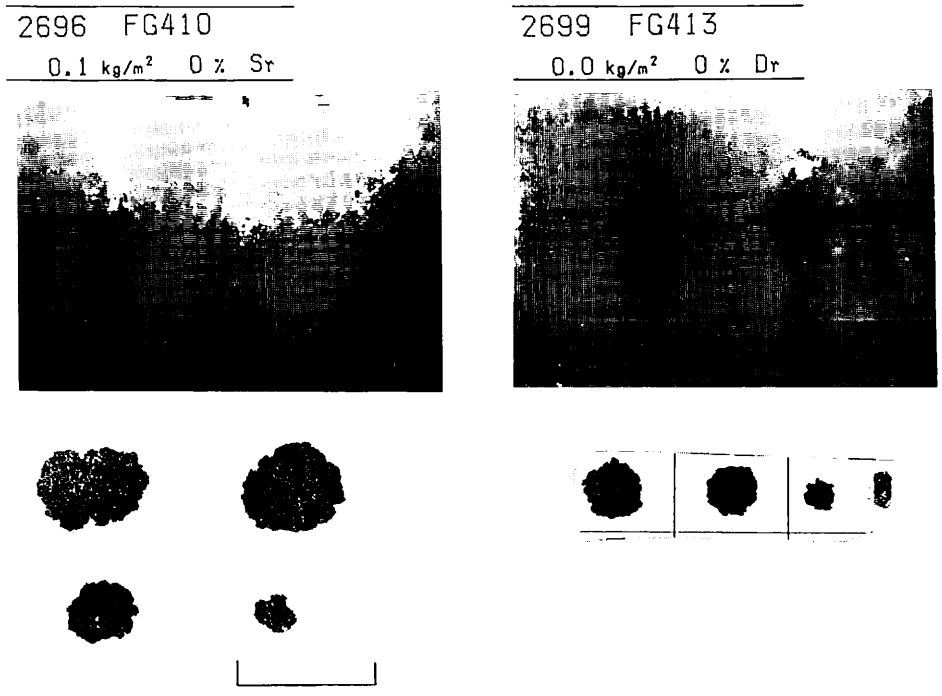

Appendix VIII-2(40)

2702 FG415

0.0 kg/m² 0 % Vr

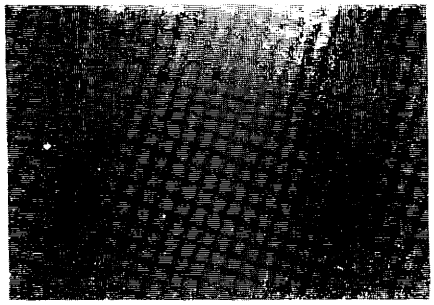

2703 FG416

0.0 kg/m² 0 % –

2704 FG417

0.0 kg/m² 0 % –

2705 B68

0.0 kg/m² 0 % Sr

box core surface

Appendix VIII-2(41)

2706 · FG418

0.1 kg/m² 0 % Sr

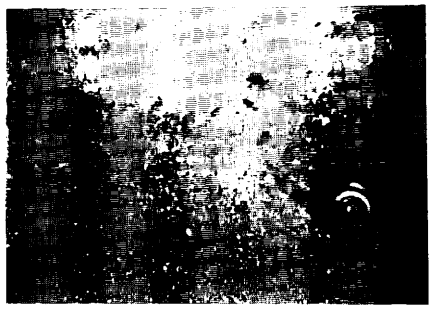

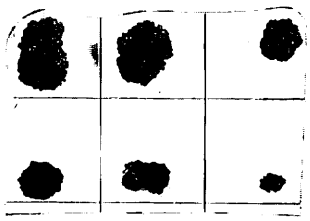

2708 FG420

0.0 kg/m² 0 % –

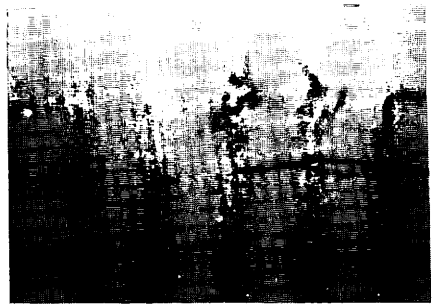

2709 FG421

0.0 kg/m² 0 % –

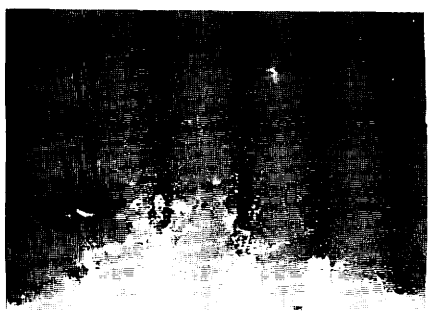

2707 FG419

0.0 kg/m² 0 % –

2710 FG422

0.2 kg/m² 0 % Dr, IDr

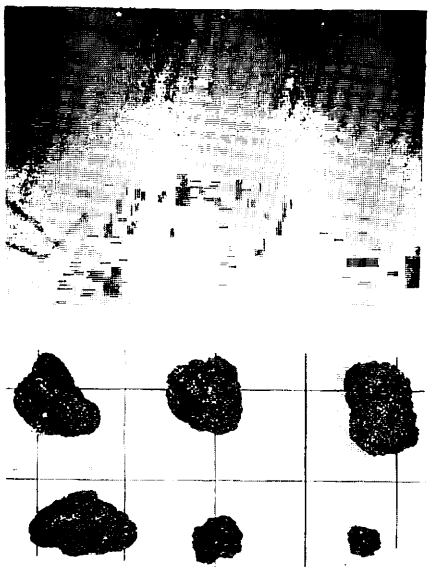

2711 FG423

9.6 kg/m² 7 % IDsr, IDPsr

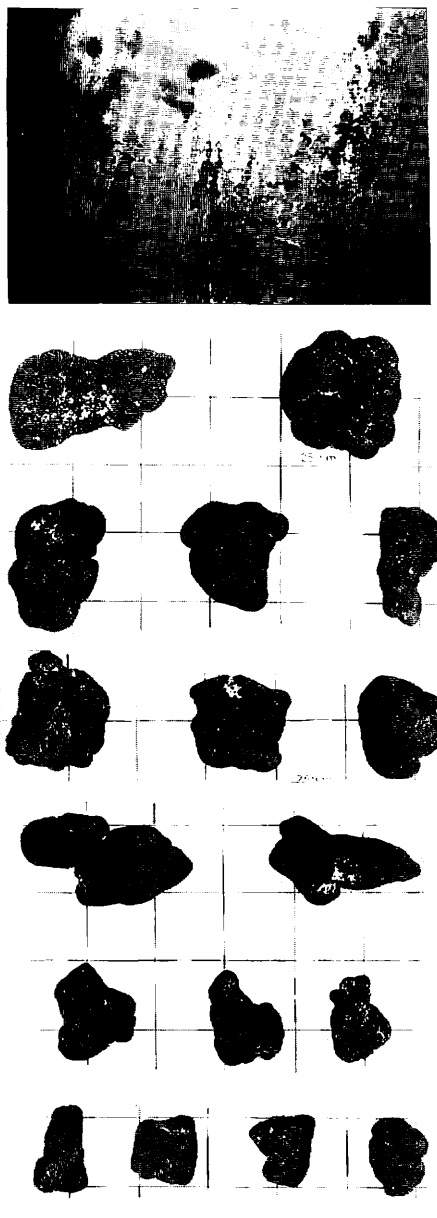

2712 P229

- - IDr, IDPr

Appendix VIII-2(43)

Appendix VIII-3 Manganese nodules buried deep within piston cores and box cores.

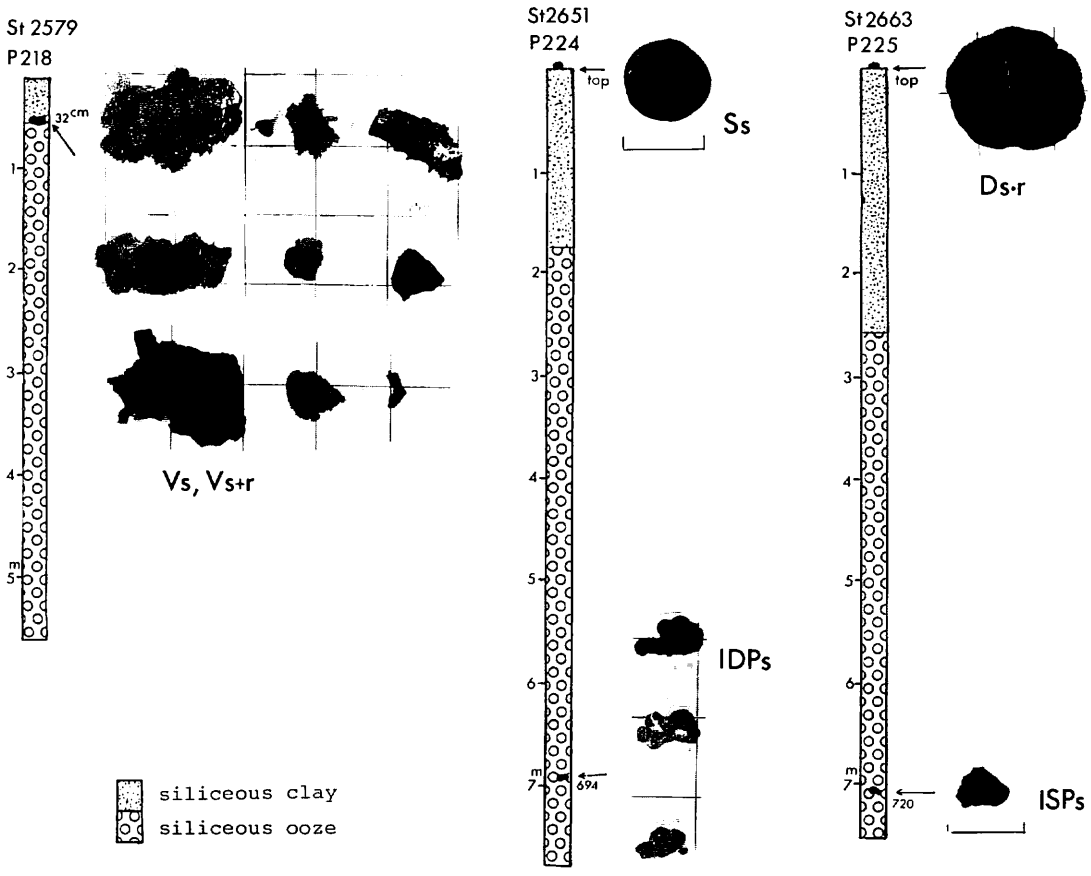

Appendix VIII-3(1)

St 2645 B63

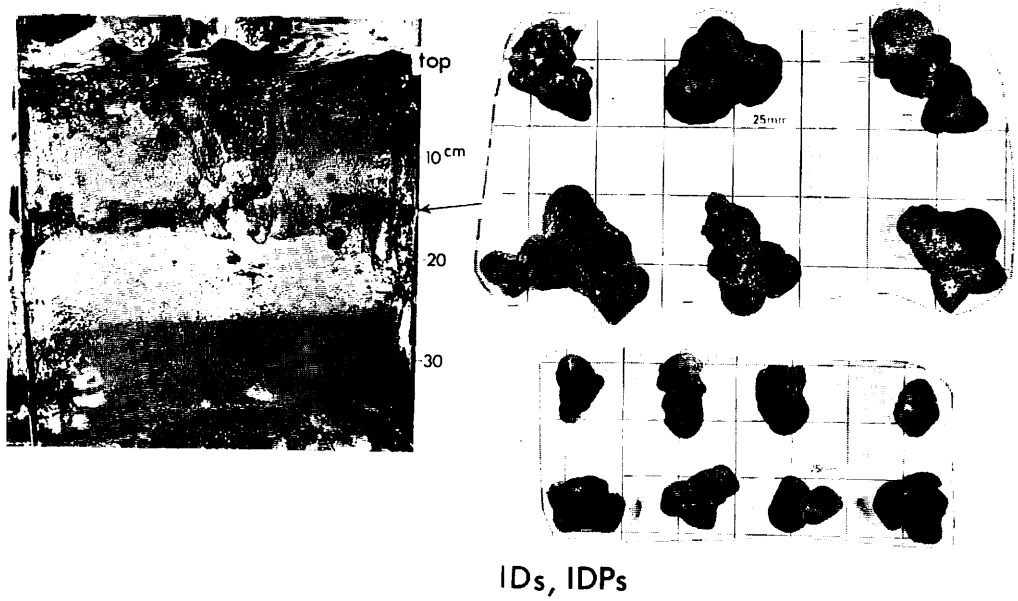

Appendix VIII-3(2)